РОССИЙСКАЯ АКАДЕМИЯ НАУК
Институт проблем безопасного развития атомной энергетики

RUSSIAN ACADEMY OF SCIENCES
Nuclear Safety Institute (IBRAE)

Simulation of the oxide layer growth on the surface of stainless steel in heavy-liquid metal with help of the EUKLID/V2 code

Spokesperson: Usov E.V.

Kudasov I.G., Mosunova N.A., Sorokin A.A., Chukhno V.I.

The goals of the work

Development of the EUKLID/V2 code to simulate the processes of oxide layer formation, transfer of the corrosion and fission products in heavy liquid metal

It is necessary to create mathematical models to:

- Simulate the growth and destruction of the oxide layer
- Oxygen and iron oxide transfer in liquid metal coolant
- Impurity coagulation
- Sedimentation of the impurities on the wall

The basic processes

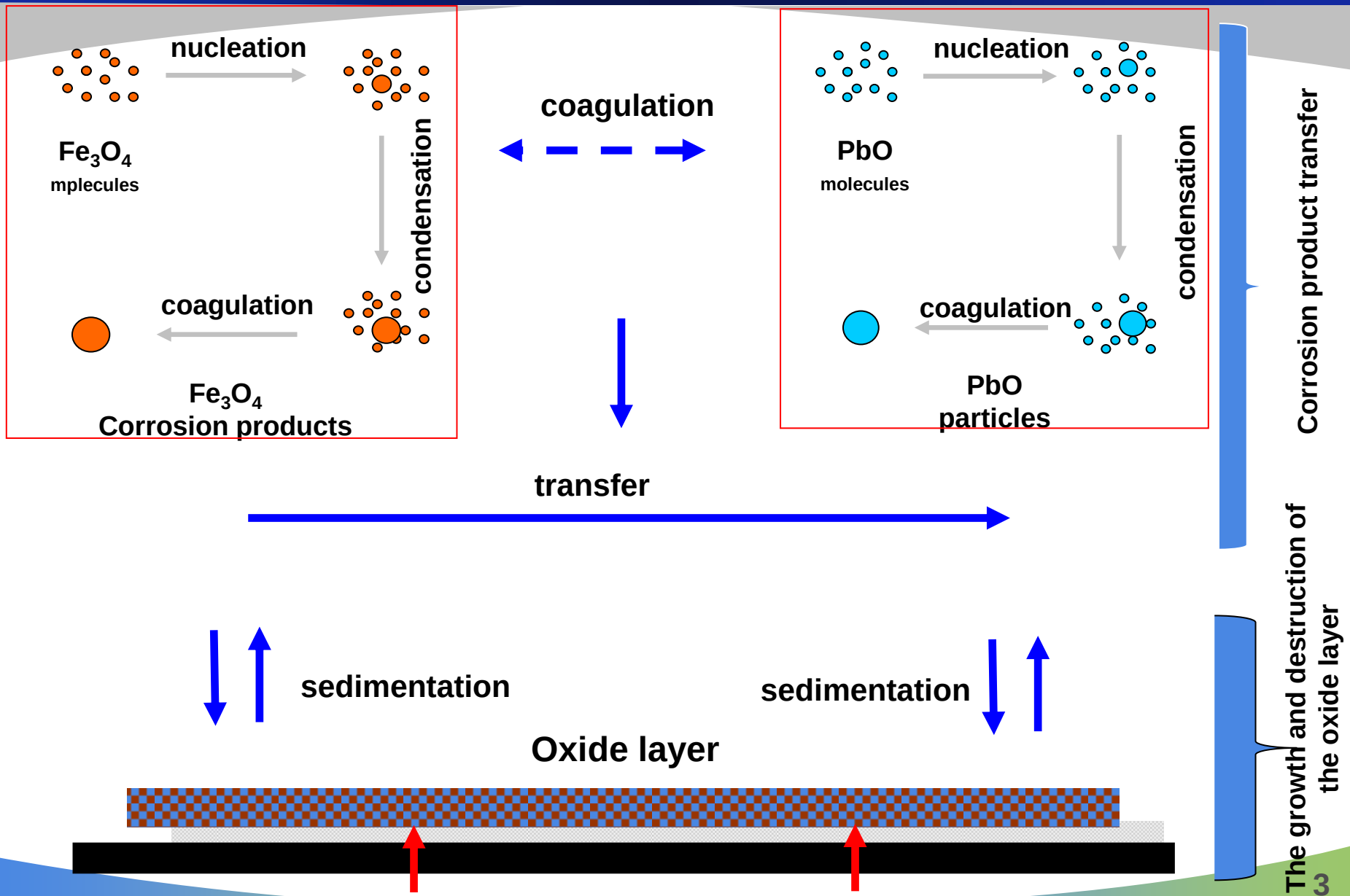

Oxide layer formation. Two-layer model

In the proposed model, the main dynamic variables are the thickness of the layers of Fe_3O_4 and iron-chromic spinel $Fe_{3-x}Cr_xO_4$

$$^{*}\begin{cases} \rho_{ox}\dfrac{d\delta_m}{dt} = J_{Fe}^{ox} + J_{O}^{ox} - k_{rem}, \\ \rho_{s}\dfrac{d\delta_s}{dt} = J_{O}^{s} + J_{Fe}^{s} + J_{Cr}^{s}, \end{cases}$$

Where $^{**}k_{rem}$ the rate of erosion, δ_m - the thickness of the Fe_3O_4 layer, the thickness of the $Fe_{3-x}Cr_xO_4$ - layer

*V.V. Alekseev, E.A. Orlova, F.A. Kozlov, I.Yu. Torbenkova, A.S. Kondratyev. Calculation-theoretical analysis of the process of steel oxidation in a lead coolant // VANT, ser .: Nuclear constants, vol. 1-2, 2010, p. 56-66. (In Russian)
**Mikityuk K. Analytical model of the oxide layer build-up in complex lead-cooled systems // Nuclear Engineering Design, Vol. 240. – Pp.3632-3637, 2010.

Two-layer model

In accordance to the model the diffusion flow that forms the layers can be calculated:

$$J_O^{ox} = J_O^T - J_O^{difm}, \quad J_{Fe}^{ox} = J_{Fe}^{difm} - J_{Fe}^T,$$

$$J_O^s = J_O^{difm}, \quad J_{Cr}^s = J_{Cr}^{difs},$$

$$J_{Fe}^s = J_{Fe}^{difs} - J_{Fe}^{difm}.$$

In accordance to the chemical reaction :

$$J_O^{ox} = \frac{4m_O}{3m_{Fe}} J_{Fe}^{ox}, \; J_O^s = \frac{4m_O}{2.64m_{Fe}} J_{Fe}^s, \; J_O^s = \frac{4m_O}{0.36m_{Cr}} J_{Cr}^s;$$

$$3Fe + 4PbO \Leftrightarrow Fe_3O_4 + 4Pb, \quad a_O^w = \left[K_{eq}^{ox}\left(a_{Fe}^w\right)^3\right]^{-1/4}, \; K_{eq}^{ox} = \exp\left(-\frac{\Delta G_R^{ox}}{RT}\right), \; \Delta G_R^{ox} = \Delta G_{Fe_3O_4}^0 - 4\Delta G_{PbO}^0,$$

$$Fe + 2Cr + 4O \Leftrightarrow FeCr_2O_4, \; a_O^s = \left[K_{eq}^s a_{Fe}^s \left(a_{Cr}^s\right)^2\right]^{-1/4},$$

$$K_{eq}^s = \exp\left(-\frac{\Delta G_R^s}{RT}\right), \; \Delta G_R^s = \Delta G_{FeCr_2O_4}^0 \quad {}^*\Delta G_R^{ox} = -292100 + 0,6T,$$

$${}^*\Delta G_R^s = -574330 - 69.6T;$$

*V.V. Alekseev, E.A. Orlova, F.A. Kozlov, I.Yu. Torbenkova, A.S. Kondratyev. Calculation-theoretical analysis of the process of steel oxidation in a lead coolant // VANT, ser .: Nuclear constants, vol. 1-2, 2010, p. 56-66. (In Russian)

Corrosion products transfer. Upwind scheme

$$\frac{\partial C}{\partial t} + v\frac{\partial C}{\partial z} = 0$$

Upwind scheme

$$\frac{C_i^{n+1} - C_i^n}{\tau} + v\frac{C_i^n - C_{i-1}^n}{\Delta z} = 0$$

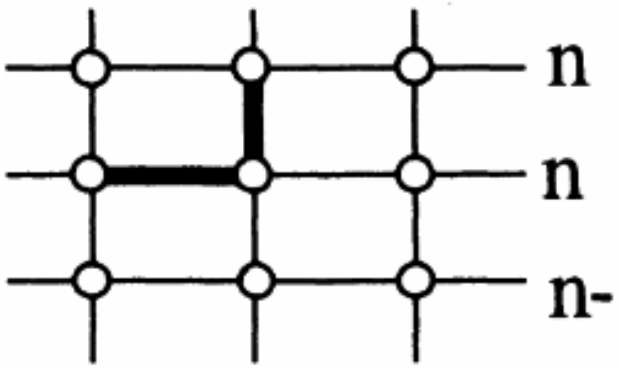

Advantages:

- Monotone difference scheme
- CFL-condition

Disadvantages:

- High numerical diffusion

$$\frac{\partial C}{\partial t} + v\frac{\partial C}{\partial z} = 0 \Rightarrow \frac{C_i^{n+1} - C_i^n}{\tau} = -v\frac{\partial C}{\partial z} + \frac{v\Delta z}{2}\frac{\partial^2 C}{\partial^2 z}$$

High-order accuracy difference scheme. CABARET-scheme

Advantages:

- Low numerical diffusion

Disadvantages:

- Two-order numerical accuracy

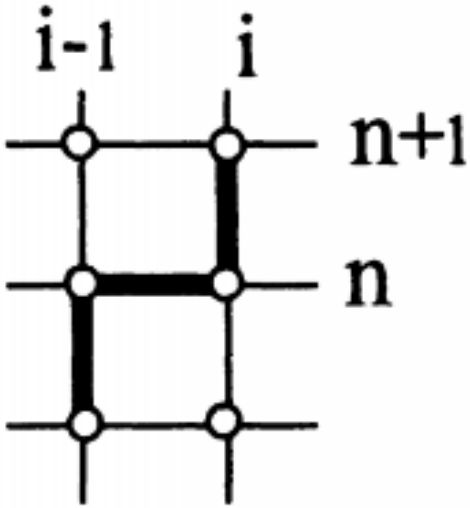

Numerical method

*

$$\frac{C_i^{n+1}-C_i^n}{\tau}+v\frac{C_i^n-C_{i-1}^n}{\Delta z}+Q_{i-1}=0$$

$$\tilde{C}_i=(1-r)C_i^n+rC_{i-1}^n-\tau Q_{i-1},\ r=\frac{\tau v}{\Delta z},$$

$$Q_{i-1}=\frac{C_{i-1}^n-C_{i-1}^{n-1}}{\tau}+v\frac{C_i^n-C_{i-1}^n}{h}$$

$$C_i^{n+1}=\begin{cases} C_i^{max},\ \tilde{C}_i>C_i^{max}; \\ \tilde{C}_i; \\ C_i^{min},\ \tilde{C}_i<C_i^{min}; \end{cases}$$

*V. M. Goloviznin, S. A. Karabasov. Nonlinear correction of Cabaret scheme// Matem. Mod., Vol. 10, Number 12,1998.

Calculation of coagulation

Coagulation equation:

$$\frac{\partial C}{\partial t} = L_{coag}(v) + S(v,t) - R(v,t)\,\mathrm{C} + L_{cond}(v)$$

$$L_{coag}(v) = \frac{1}{2}\int_0^v K(u, v-u)\,\mathrm{C}(u,t)\,\mathrm{C}(v-u,t)\,du - C(v,t)\int_0^\infty K(v,u)\,\mathrm{C}(u,t)\,du$$

Numerical scheme:

$$\begin{cases} \dfrac{dN_i}{dt} = \left(\dfrac{m_{ox}}{m_i - m_{i-1}}\right)\left[K_{i-1}N_{i-1}N_{ox} - E_i N_i\right] - \left(\dfrac{m_{ox}}{m_{i+1} - m_i}\right)\left[K_i N_i N_{ox} - E_{i+1}N_{i+1}\right] + \\ \quad + N_{i-1}\displaystyle\sum_{j=1}^{i-1} f_{i-1,j}\left(\dfrac{m_j}{m_i - m_{i-1}}\right)K_{i-1,j}N_j - N_i\sum_{j=1}^{i-1} f_{ij}\left(\dfrac{m_j}{m_{i+1} - m_i}\right)K_{i,j}N_j - N_i\sum_{j=i+1}^{j\max} K_{i,j}N_j - \\ \quad - N_i\displaystyle\sum_{jc=1}^{j\max} K_{i,jc}^{corr}N_{jc}, \\ \dfrac{dN_{ox}}{dt} = \displaystyle\sum_i E_i N_i - N_{ox}\sum_i K_i N_i \end{cases}$$

Cousin F., Dieschbourg K., Jacq F. New capabilities of simulating fission product transport in circuits with ASTEC/SOPHAEROS v.1.3. Nuclear Engineering and Design, 238, 2430-2438, 2008.

Coagulation. Analytical test

Coagulation equation:

$$\frac{\partial}{\partial t}C(u,t)=\frac{K_0}{2}\int_0^u \mathrm{C}(v,t)C(u-v,t)dv-K_0\,\mathrm{C}(u,t)\int_0^\infty \mathrm{C}(v)dv,$$

Initial distribution

$$n(v,0)=\frac{N_0}{v_0}\exp\left(-\frac{v}{v_0}\right),$$

Analytical solution

$$N_i(t)=\frac{2N_0}{(\tau+2)}\left(\begin{array}{l}\exp\left(-\dfrac{2v_i}{v_0(\tau+2)}\right)-\\ -\exp\left(-\dfrac{2v_{i+1}}{v_0(\tau+2)}\right)\end{array}\right),$$

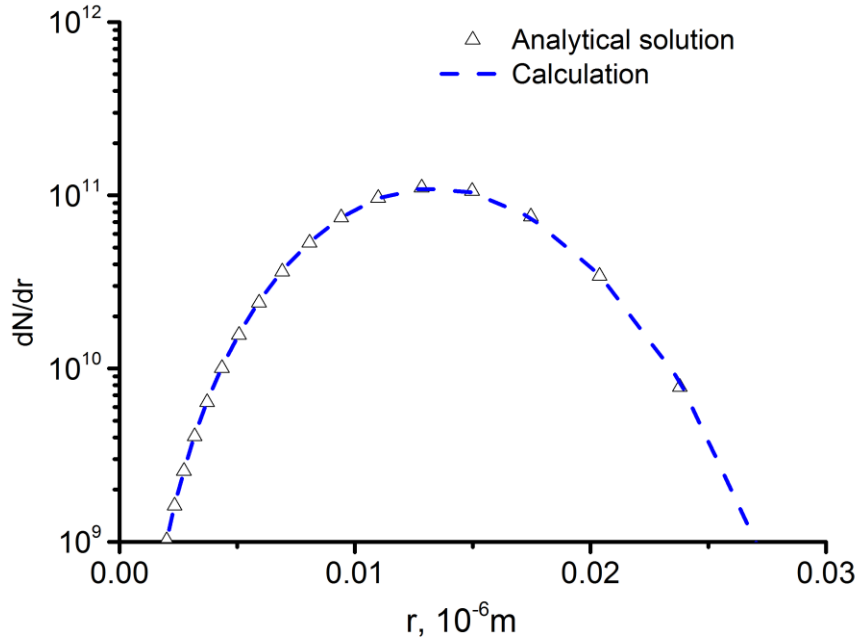

Results of calculation

Oxide layer growth. Analytical test

The basic equation:

$$\rho_{ox}\frac{d\delta}{dt} = J_{Fe}^{ox} + J_{O}^{T},$$

Diffusion flow

$$\frac{J_{O}^{T}}{4m_{O}} = \frac{J_{Fe}^{ox}}{3m_{Fe}}, \quad J_{Fe}^{ox} = J_{Fe}^{dif} - J_{Fe}^{T},$$

$$J_{Fe}^{dif} = K_{pr}\frac{a_{Fe}^{m} - a_{Fe}^{w}}{\delta}, \quad K_{pr} = 10^{-1,722-9600,0/T}$$

$$J_{Fe}^{T} = h_{Fe}C_{Fe}^{sat}(a_{Fe}^{w} - a_{Fe}^{T}),$$

$$J_{O}^{T} = h_{O}C_{O}^{sat}(a_{O}^{w} - a_{O}^{T}),$$

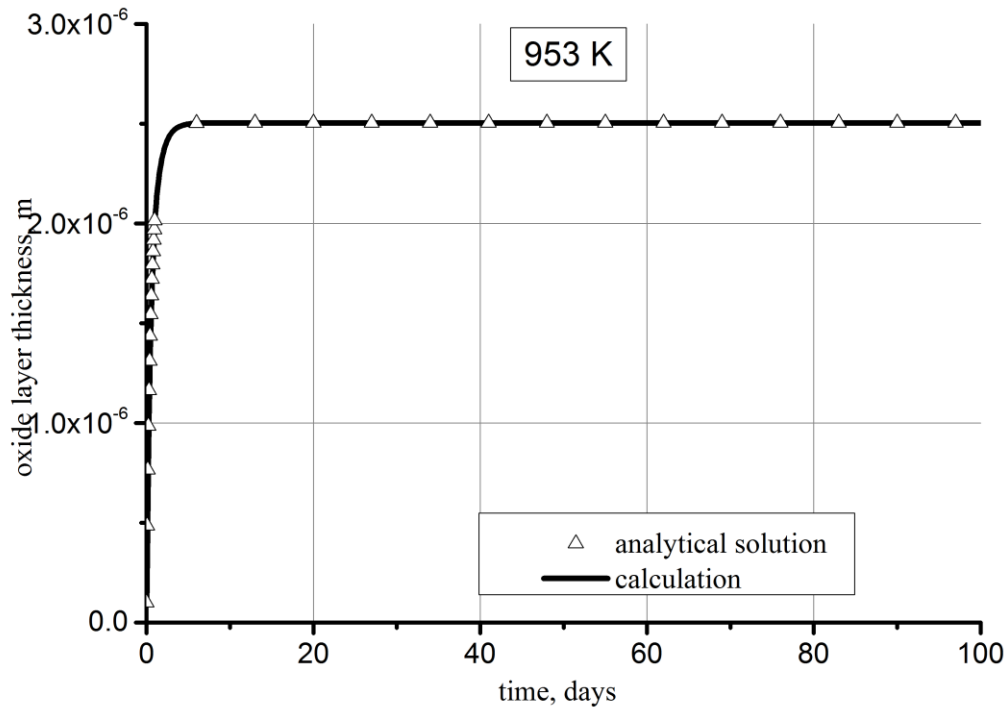

Oxide layer thickness

$$\frac{d\delta}{dt} = -\frac{da_{Fe}^{w}}{dt}\frac{K_{pr}}{\frac{3m_{Fe}}{4m_{O}}h_{O}C_{O}^{sat}\left[a_{O}^{T} - \left(K_{eq}^{ox}\left(a_{Fe}^{w}\right)^{3}\right)^{-0.25}\right] + h_{Fe}C_{Fe}^{sat}\left(a_{Fe}^{w} - a_{Fe}^{T}\right)} - \frac{da_{Fe}^{w}}{dt}\frac{K_{pr}\left(a_{Fe}^{m} - a_{Fe}^{w}\right)\left(\frac{3m_{Fe}}{4m_{O}}h_{O}C_{O}^{sat}\left[0,75\cdot\left(K_{eq}^{ox}\right)^{-0,75}\left(a_{Fe}^{w}\right)^{-1.25}\right] + h_{Fe}C_{Fe}^{sat}\right)}{\left(\frac{3m_{Fe}}{4m_{O}}h_{O}C_{O}^{sat}\left[a_{O}^{T} - \left(K_{eq}^{ox}\left(a_{Fe}^{w}\right)^{3}\right)^{-0.25}\right] + h_{Fe}C_{Fe}^{sat}\left(a_{Fe}^{w} - a_{Fe}^{T}\right)\right)^{2}}$$

Simulation of experiment on the oxide layer growth(Glasbrenner)

Inaccuracy of the initial data

Parameters	error, %
Coolant velocity, %	±5
Lead temperature, %	±5
Coolant pressure, %	±3
Oxygen concentration in coolant, %	±2

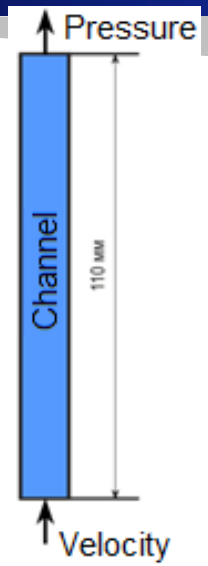

V=1,9 m/s,
T=550 ^{0}C
D_in= 8 mm
D_out=30 mm

Sensitivity coefficient

Parameters	Sensitivity coefficient
Coolant velocity	0.000
Lead temperature	**0.993**
Coolant pressure	-0.009
Oxygen concentration in coolant	-0.015

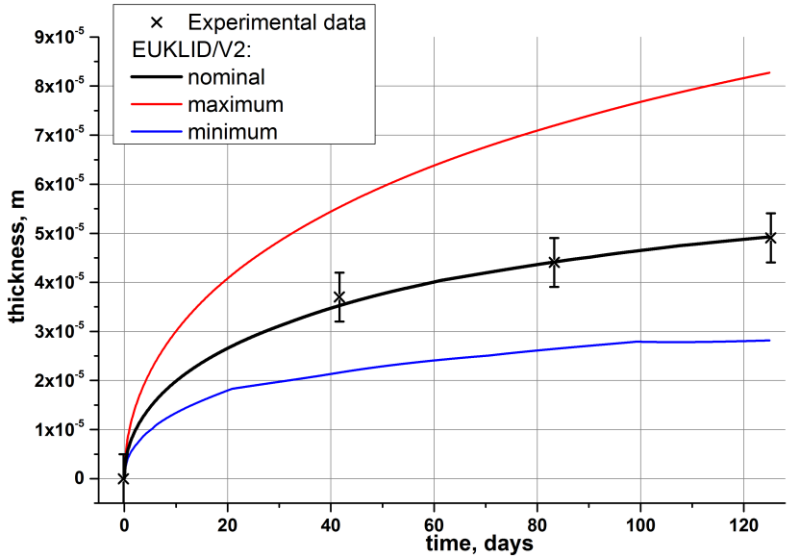

Oxide layer thickness

H Glasbrenner, J Konys, G Mueller, A Rusanov, Corrosion investigations of steels in flowing lead at 400°C and 550°C. // Journal of Nuclear Materials. v. 296. i. 1. 2001. pp. 237-242.

Simulation of experiment on the oxide layer growth(IPPE)

Inaccuracy of the initial data

Parameters	error, %
Velocity, %	±5
Lead temperature, %	±3
Cr concentration in stainless steel, %	±2
Oxygen concentration in coolant, %	±2

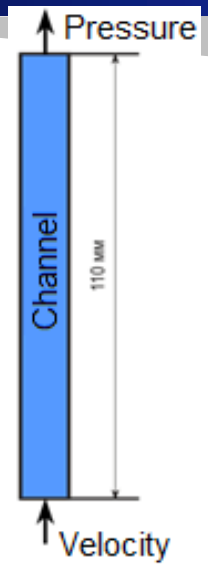

V=1,7 m/s,
T=923 K
D= 10 mm

Sensitivity coefficient

Parameters	Sensitivity coefficient
Velocity	-0,0990
Lead temperature	-0,084
Cr concentration in stainless steel	**-0,158**
Oxygen concentration in coolant	0,0915

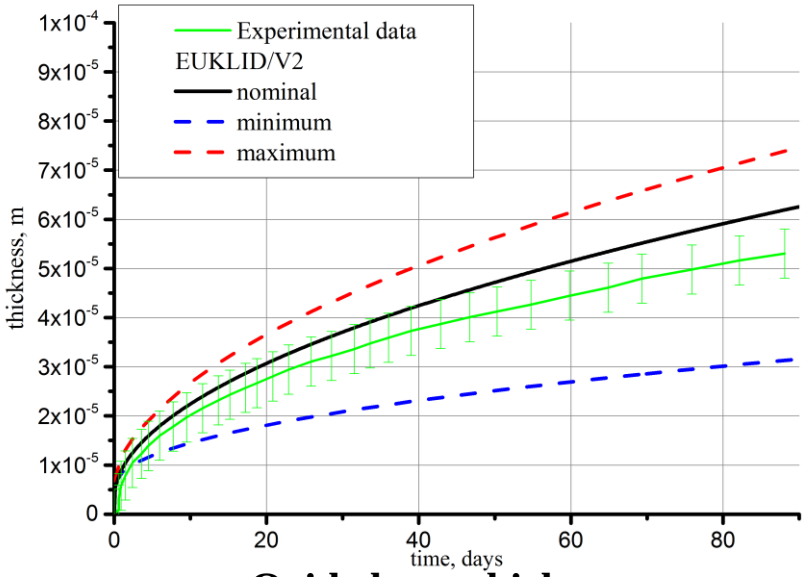

Oxide layer thickness

*V.V. Alekseev, E.A. Orlova, F.A. Kozlov, I.Yu. Torbenkova, A.S. Kondratyev. Calculation-theoretical analysis of the process of steel oxidation in a lead coolant // VANT, ser .: Nuclear constants, vol. 1-2, 2010, p. 56-66. (In Russian)

Simulation of experiment on the oxide layer growth (Pb-Bi)

Inaccuracy of the initial data

Parameters	error, %
Velocity, %	±5
Lead-Bismuth temperature, %	±5
Pressure, %	±3
Oxygen concentration in coolant, %	±2

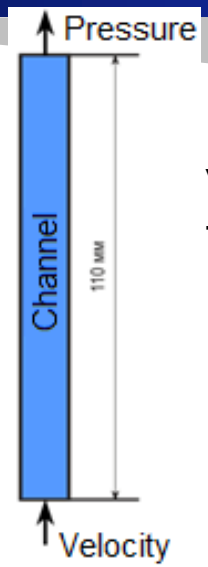

V=1,2 m/s,
T=803 K
D= 1,8 mm

Коэффициенты чувствительности толщины оксидного слоя по отношению к изменению варьируемых параметров

Parameters	Коэффициент чувствительности
Velocity, %	-0,175
Lead-Bismuth temperature, %	**0,615**
Pressure, %	-0,24
Oxygen concentration in coolant, %	-0,068

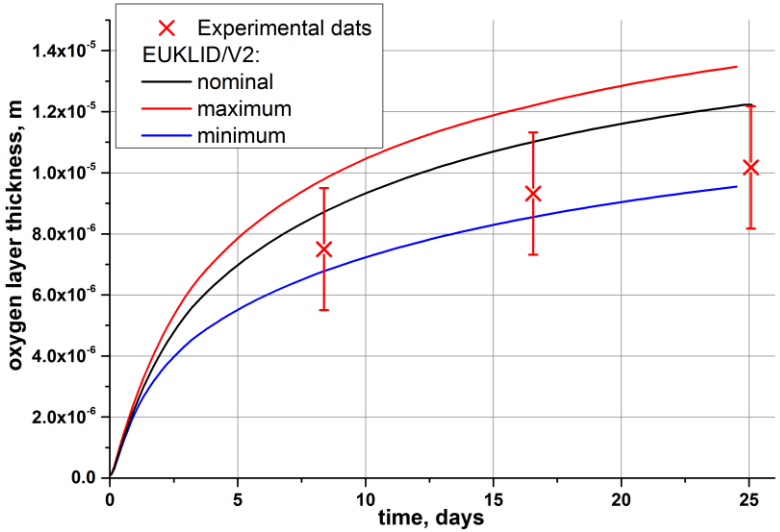

Oxide layer thickness

Machut M., K. Sridharan, N. Li, S. Ukai, T. Allen. Time dependence of corrosion in steels for use in lead-alloy cooled reactors. Journal of Nuclear Materials. // Journal of Nuclear Materials. v. 371. i. 1–3. 2007. pp. 134-144.

Conclusion

- The module of oxygen layer growth has been created as a part of coupled code EUKLID/V2
- The module contains the models of oxygen layer growth and destruction, models of coagulation and transfer of corrosion products
- The result of analytical test calculation and simulation of experiments has been presented

РОСАТОМ

ГНЦ РФ – ФЭИ

METHODOLOGY OF PROCESSING EXPERIMENTAL DATA ON STEEL OXIDATION KINETICS IN HLMC EXEMPLIFIED BY PEARLITIC STEEL EP 79 IN LEAD-BISMUTH

AUTHORS: O.V. Lavrova, K.D. Ivanov, A.Yu. Legkikh

V international conference
Heavy liquid metal coolant in nuclear technologies
(HLMC-2018)
8-10 October 2018 Obninsk, Russia

Considered steel

Grade of considered steel : **ЭП 79 (15ХСМФБ)**

Chemical composition

Component	Cr	Ni	Si	C	Mn	S	P
Concentration, % wt.	1.41	0.14	0.89	0.15	0.32	0.005	0.007

Component	Nb	V	B	Mo	W	Ti	Al	N
Concentration, % wt.	0.25	0.24	-	0.51	-	0.1	0.03	-

Environment in which the oxidation of steel was carried out: lead-bismuth

The conditions and results of oxidation of the steel samples

№ test	t, ^{0}C	τ, hour	C, % wt.	δ, µm	Test facility
1	620; 550; 390	400	~ $2\cdot 10^{-6}$	35 – 40; 15 – 20; ~ 2	SIP
2	620; 570; 450	400	~ $5\cdot 10^{-5}$	70 – 80; ~ 30; ~ 6	SIP
3	620; 580 ; 350	400	~ $1\cdot 10^{-7}$	8 – 10; ~ 10; ~ 1	SIP
4	450	790	~ $1\cdot 10^{-7}$	2 - 3	CU-2M
5	580; 400	1500	~ $2\cdot 10^{-6}$	~ 30; ~ 3	CU-2M
6	550; 450	1230	$(1\div 2)\cdot 10^{-6}$	~ 16; ~ 4	SVR
7	570; 510; 390	2300	$(1\div 2)\cdot 10^{-6}$	~ 40; ~ 20; ~6	CU-1M
8	570; 510; 390	2500	$4\cdot 10^{-6} \div 8\cdot 10^{-7}$	25 – 35; 18 – 20; ~ 2	CU-1M
9	600; 510; 410	2100	$(1\div 2)\cdot 10^{-6}$	~ 10; ~ 20; ~ 6	CU-1M
10	465; 270	3140	~ $5\cdot 10^{-7}$	~ 10; 1 - 2	SIP
11	620; 580	400	~ $1\cdot 10^{-7}$	~ 25; ~ 10	CU-2M
12	550; 420; 350	6130	~ $8\cdot 10^{-6}$	40 – 60; 20 – 25; 12 - 15	SVR
13	620; 580; 350	2300	$1\cdot 10^{-5} \div 2\cdot 10^{-6}$	~ 80; 30 – 45; ~ 1	CU-1M
14	620; 550; 450	440	~ $2\cdot 10^{-6}$	30 – 36; 15 – 20; 6	SIP

USED BASIC LAWS AND EQUATIONS

$$\delta = \varphi(T) \cdot \vartheta(C_O) \cdot \zeta(\tau)$$

$$\ln \bar{\delta} = -\frac{A}{T} + B$$

	Oxidation laws	Coordinate for linearization
Simple parabolic law	$\delta = \kappa \tau^{\frac{1}{2}}$	$\ln\delta = f(\ln\tau)$
Complex parabolic law	$a\delta^2 + в\delta = c\tau$	$\tau/\delta = f(\delta)$
Power law	$\delta = a\tau^n$	$\ln\delta = f(\ln\tau)$

Operation to expand the experimental data matrix

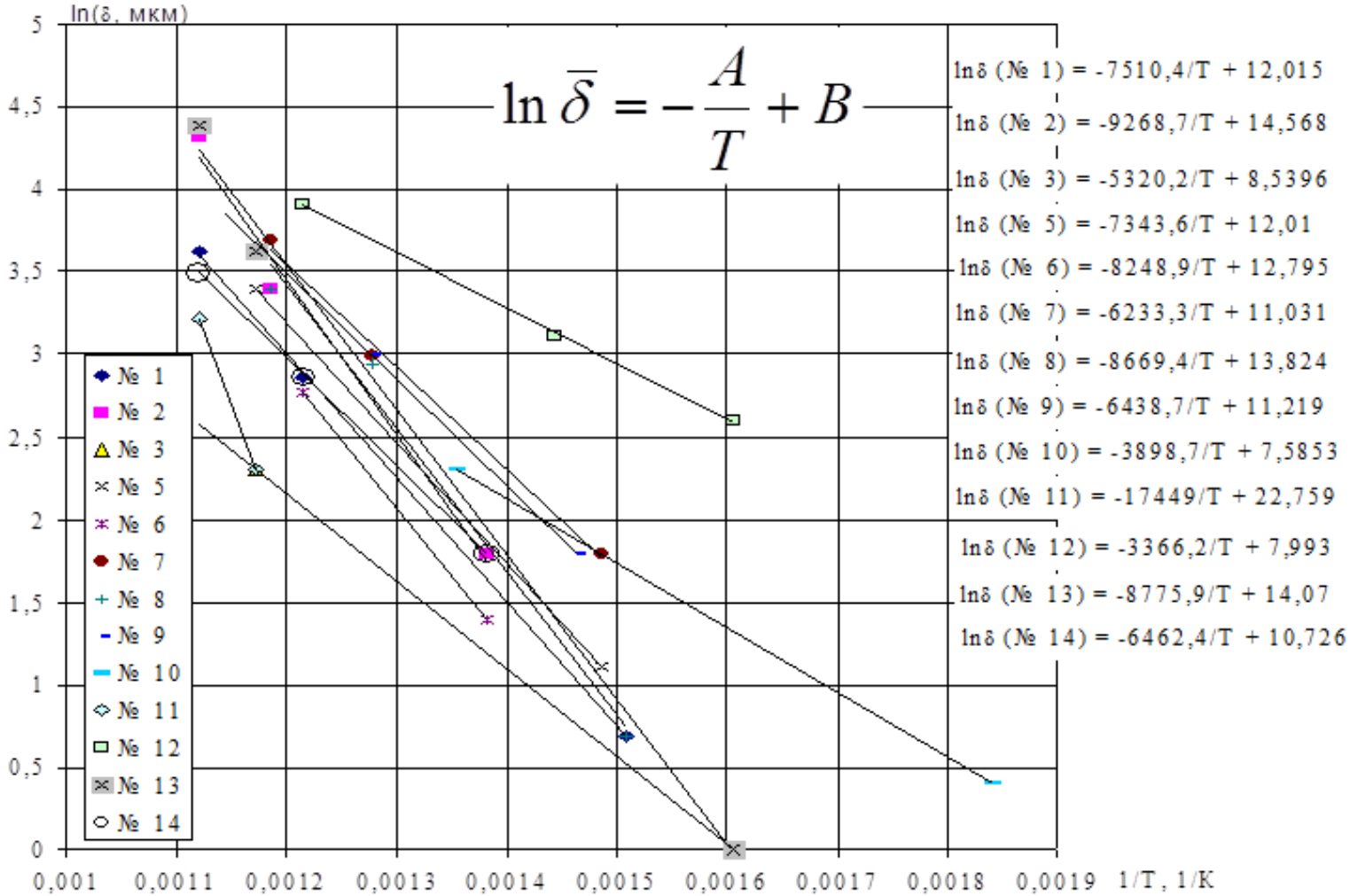

The dependence of the experimental thickness of the oxide film on the temperature in different experiments

Treatment of the expanded matrix according to the complex-parabolic law of oxidation kinetics

ГНЦ РФ – ФЭИ

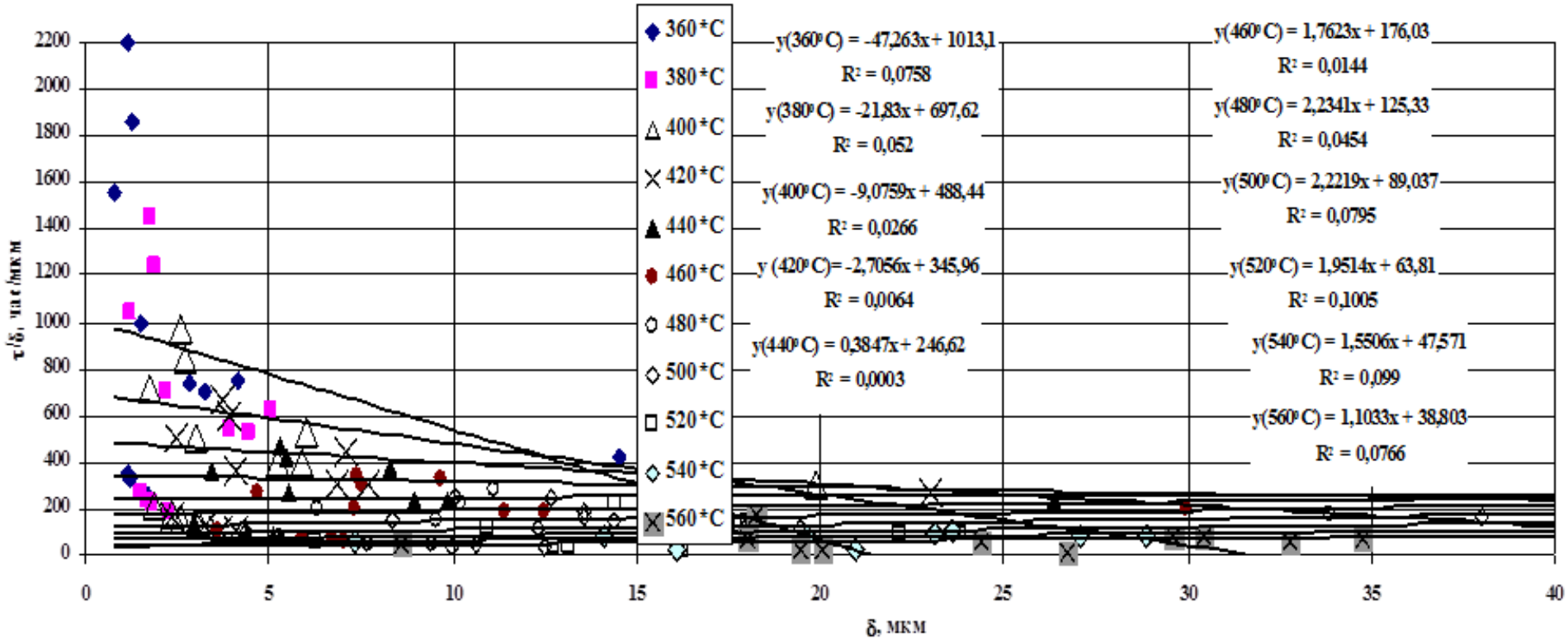

Verification of conformity of oxidation kinetics of steel EP 79 in melt lead-bismuth to the complex parabolic law

$$a\delta^2 + в\delta = c\tau$$

Treatment of the expanded matrix according to the power law of oxidation kinetics

ГНЦ РФ – ФЭИ

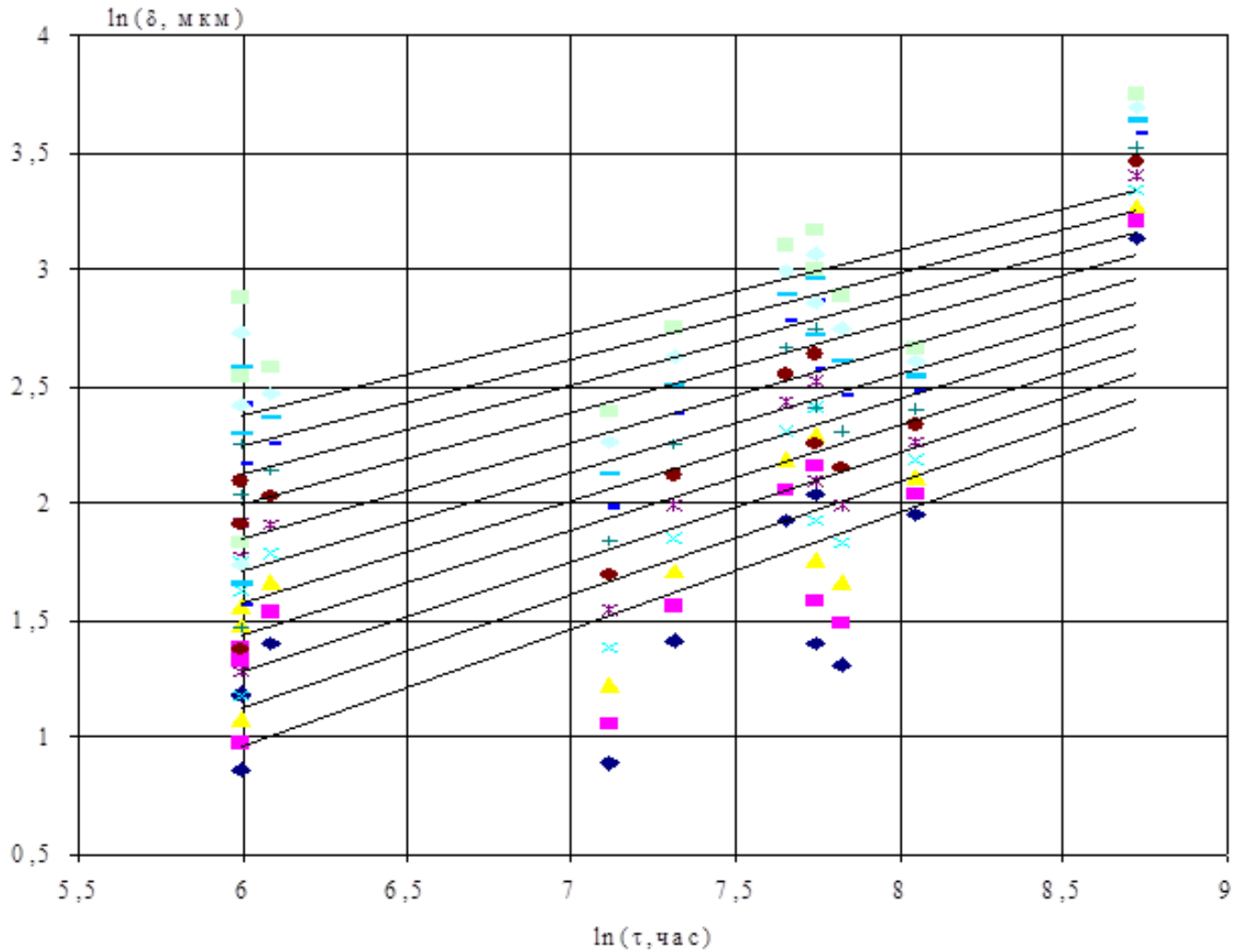

$y\,(420^0C) = 0{,}4962x - 2{,}005$
$R^2 = 0{,}5578$

$y\,(430^0C) = 0{,}4802x - 1{,}7508$
$R^2 = 0{,}5679$

$y\,(440^0C) = 0{,}4647x - 1{,}5036$
$R^2 = 0{,}5758$

$y\,(450^0C) = 0{,}4496x - 1{,}2633$
$R^2 = 0{,}5811$

$y\,(460^0C) = 0{,}4349x - 1{,}0296$
$R^2 = 0{,}5832$

$y\,(470^0C) = 0{,}4206x - 0{,}8022$
$R^2 = 0{,}5817$

$y\,(480^0C) = 0{,}4067x - 0{,}5808$
$R^2 = 0{,}5762$

$y\,(490^0C) = 0{,}3931x - 0{,}3652$
$R^2 = 0{,}5664$

$y\,(500^0C) = 0{,}3799x - 0{,}1552$
$R^2 = 0{,}5522$

$y\,(520^0C) = 0{,}3671x + 0{,}0495$
$R^2 = 0{,}5337$

$y\,(530^0C) = 0{,}3545x + 0{,}249$
$R^2 = 0{,}5113$

Processing of the extended matrix according to the power law $\delta = a\tau^n$

Temperature parameters of the power low

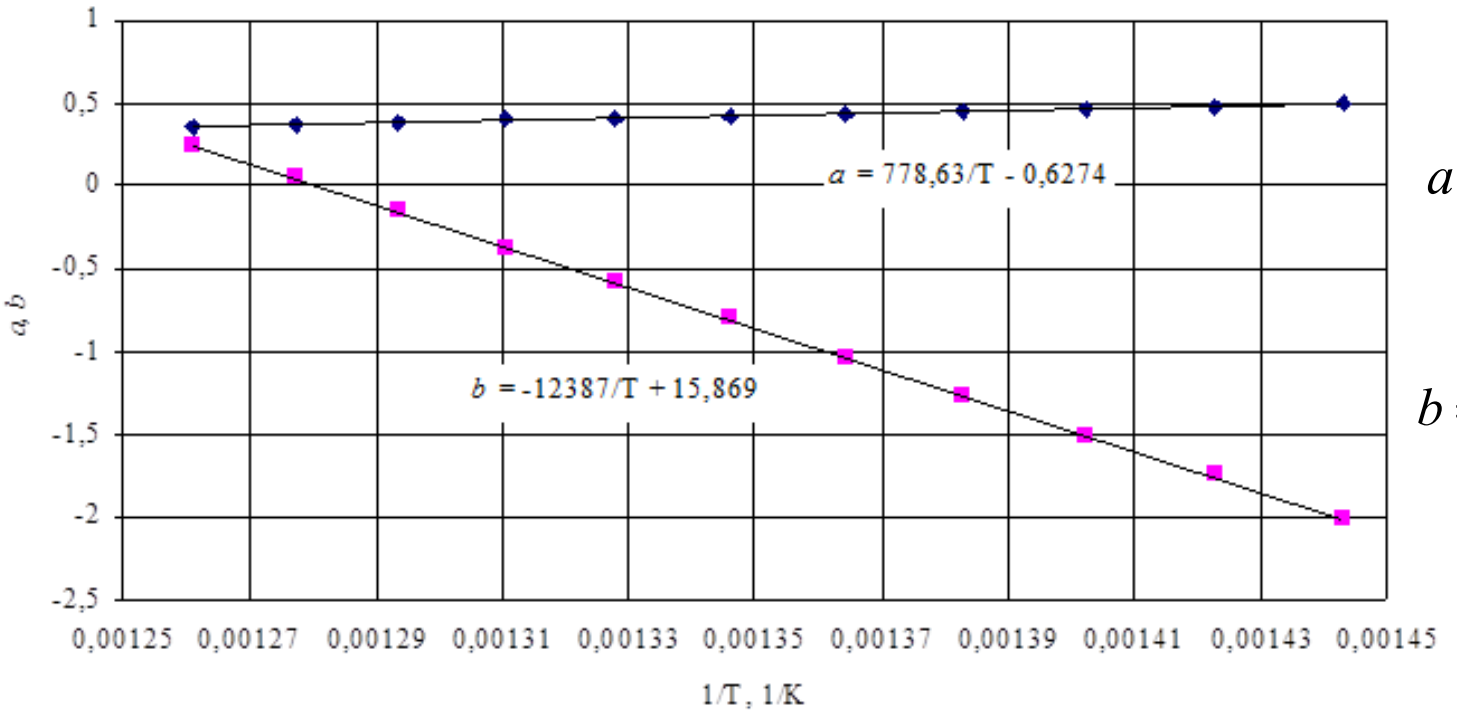

$$a = \frac{778{,}63}{T} - 0{,}6274$$

$$b = -\frac{12387}{T} + 15{,}869$$

Temperature parameters of a linear equation
lnδ = a·lnτ + b

The result of data processing

$$\ln \delta_{Calc} = -\frac{12387}{T} + 15{,}869 + \left(\frac{778{,}63}{T} - 0{,}6274\right)\ln \tau$$

Deviation of the experimental thickness of the oxide film from the calculated value depending on the oxygen concentration

ГНЦ РФ – ФЭИ

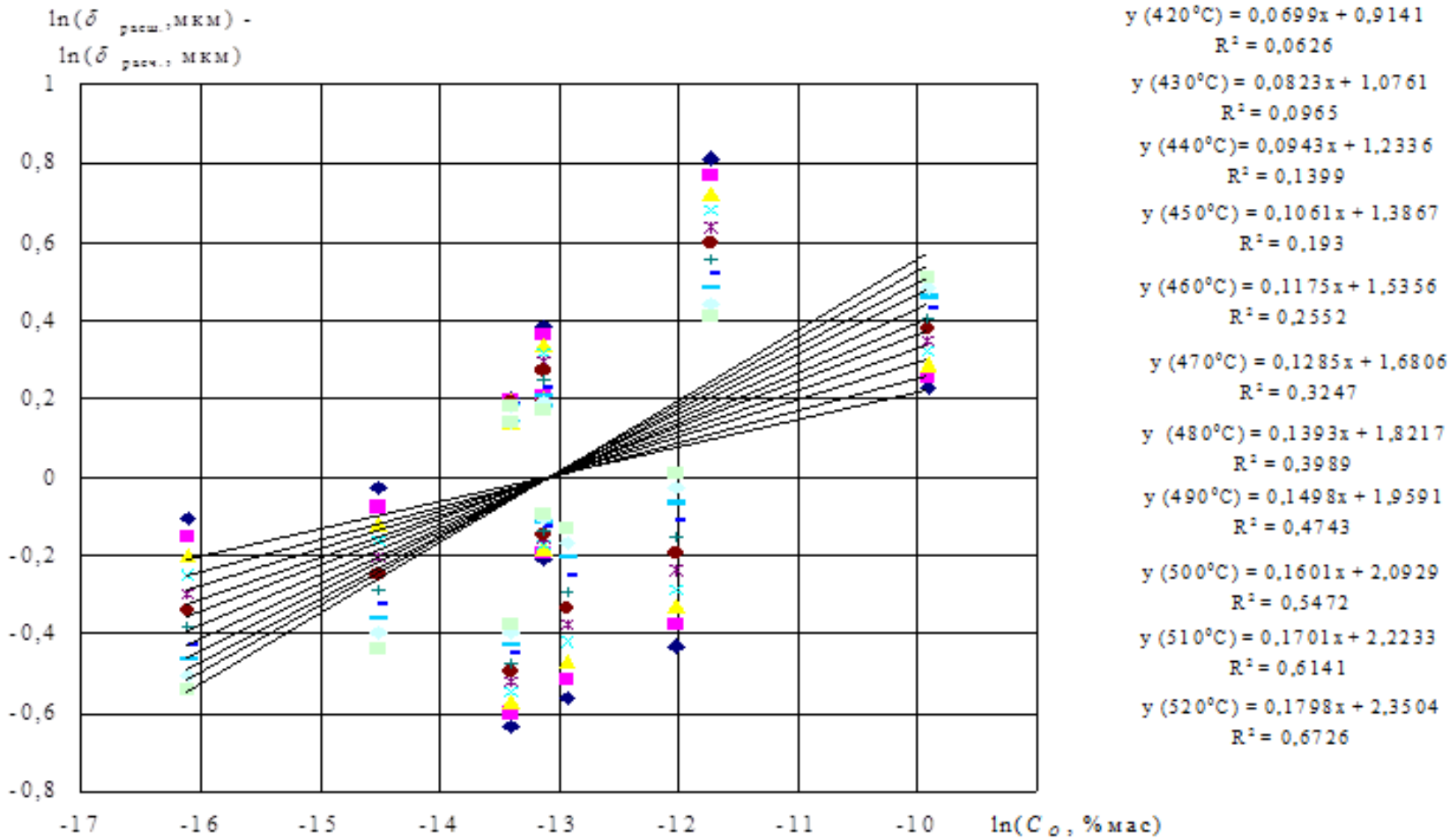

Deviations of the oxide film thickness from the calculated one depending on the oxygen regime of the coolant. The calculation was performed according to the power law

$$\ln\delta_{exp} - \ln\delta_{calc} = \phi \cdot \ln C_O + \eta$$

The temperature dependence of the parameters of a equation

$$\ln \delta_{\exp} - \ln \delta_{calc} = \varphi \ln C_O + \eta$$

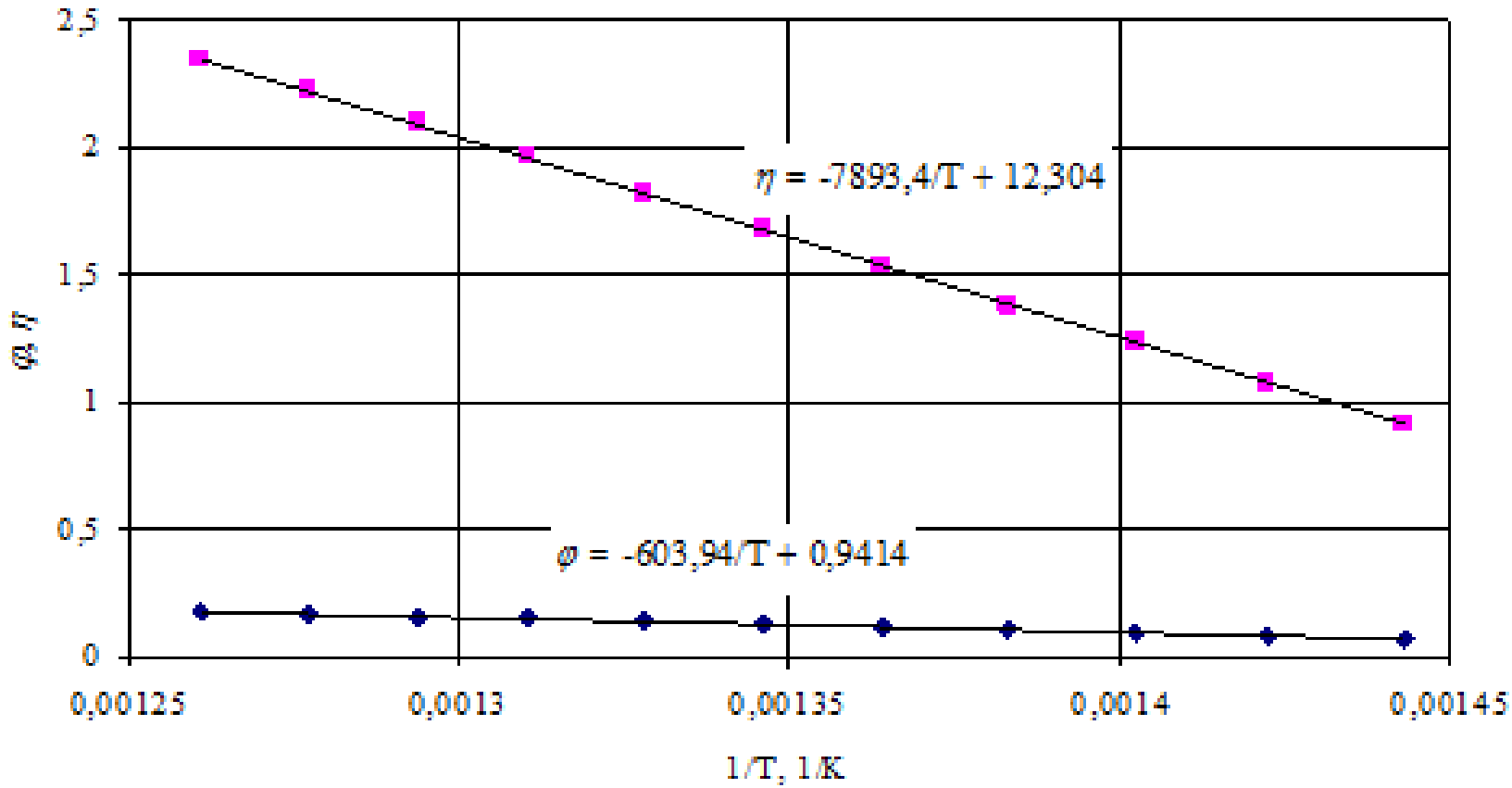

The temperature dependence of the parameters of the linear equation

$\ln(\delta_{exp}/\delta_{calc}) = \phi \cdot \ln C_O + \eta$

Compilation equation

The final calculated dependence of the oxide film thickness on the temperature, exposure time and oxygen concentration in the coolant is as follows:

$$\ln \delta_{Calc} = -\frac{20280}{T} + 28{,}173 + \left(-\frac{603{,}94}{T} + 0{,}9414\right)\ln C_O +$$

$$+\left(\frac{778{,}63}{T} - 0{,}6274\right)\ln \tau$$

Comparison of calculated and experimental data

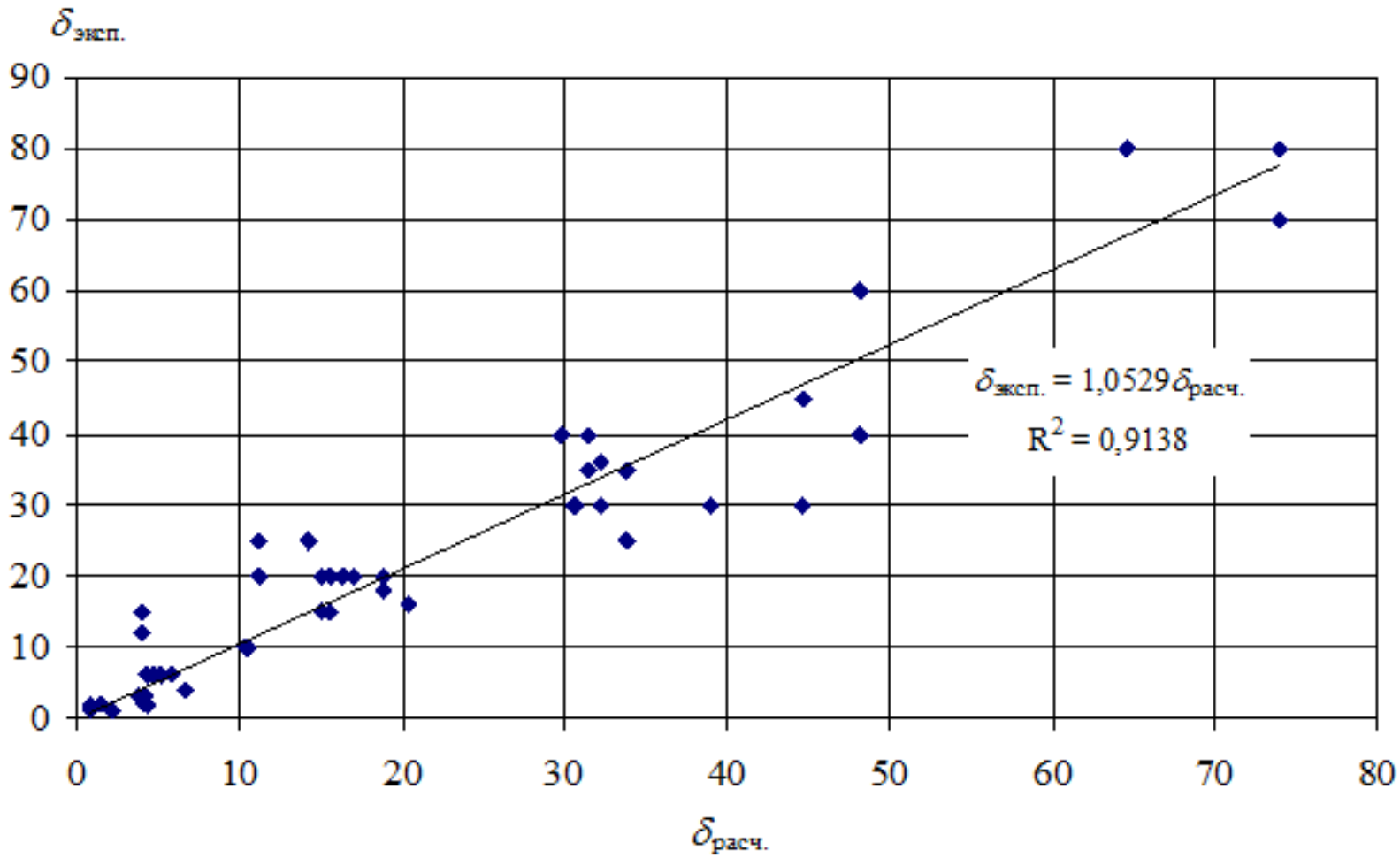

Comparison of experimental thickness of oxide films on EP 79 steel and calculated values

Conclusion

1. The proposed method made it possible to describe the data on the oxidation of low-alloy steel EP79 by the total dependence of the oxide film thickness on the temperature, exposure time and oxygen concentration in the lead-bismuth melt in a limited set of experimental data with a probability of more than 90%.

2. From the results of processing it follows that the oxidation of steel EP-79 in conditions of non-isothermal circuits with a heavy coolant in General does not obey a simple parabolic dependence. The exponent α at the time τ naturally varies with temperature according to Arrhenius's law and is α ~ of 0.62 at 350 ºC and α ~ 0,35 at 620ºC; α = ½ only when the temperature is ~ 417,6 ºC. One possible explanation for this fact is the loss of iron in the coolant at elevated temperatures and the growth of films due to the condensation of iron oxides from the coolant at low temperatures.

3. The apparent activation energy of the process varies with time and also depends on the oxygen concentration in the coolant. This indicates a change in the quality of the formed oxide coatings over time, as well as a change in the controlling stage of the mass transfer of components when the oxygen concentration changes.

4. The final calculated dependence can be used as a reference in the analysis of the results of oxidation of alloyed steels.

РОСАТОМ

ГНЦ РФ – ФЭИ

ESTIMATING THE CHANGE OF A MASS EXCHANGER PRODUCTIVITY ON ACCOUNT OF OXYGEN RESOURCE DECREASING

AUTHORS:

Radomir Askhadullin, Alexander Legkikh

V international conference

Heavy liquid metal coolant in nuclear technologies

(HLMC-2018)

8-10 October 2018 Obninsk, Russia

The role of oxygen in the heavy liquid metal technology

ГНЦ РФ – ФЭИ

To ensure the corrosion resistance of structural steels in the nuclear reactors with heavy liquid metal coolant oxygen technology is recommended. It consists in the formation of oxide films on the steel surfaces.

To preserve the integrity of the protective oxide films during the operation of nuclear reactor, it is necessary to maintain the specified oxygen regime of the coolant.

The oxygen excess in the coolant leads to the formation of slags on the heat exchange surfaces of the circuit and equipment.

Too low oxygen concentration in the coolant leads to the evolution of corrosion processes.

Forecast variation of dissolved oxygen concentration in lead coolant at reactor start-up

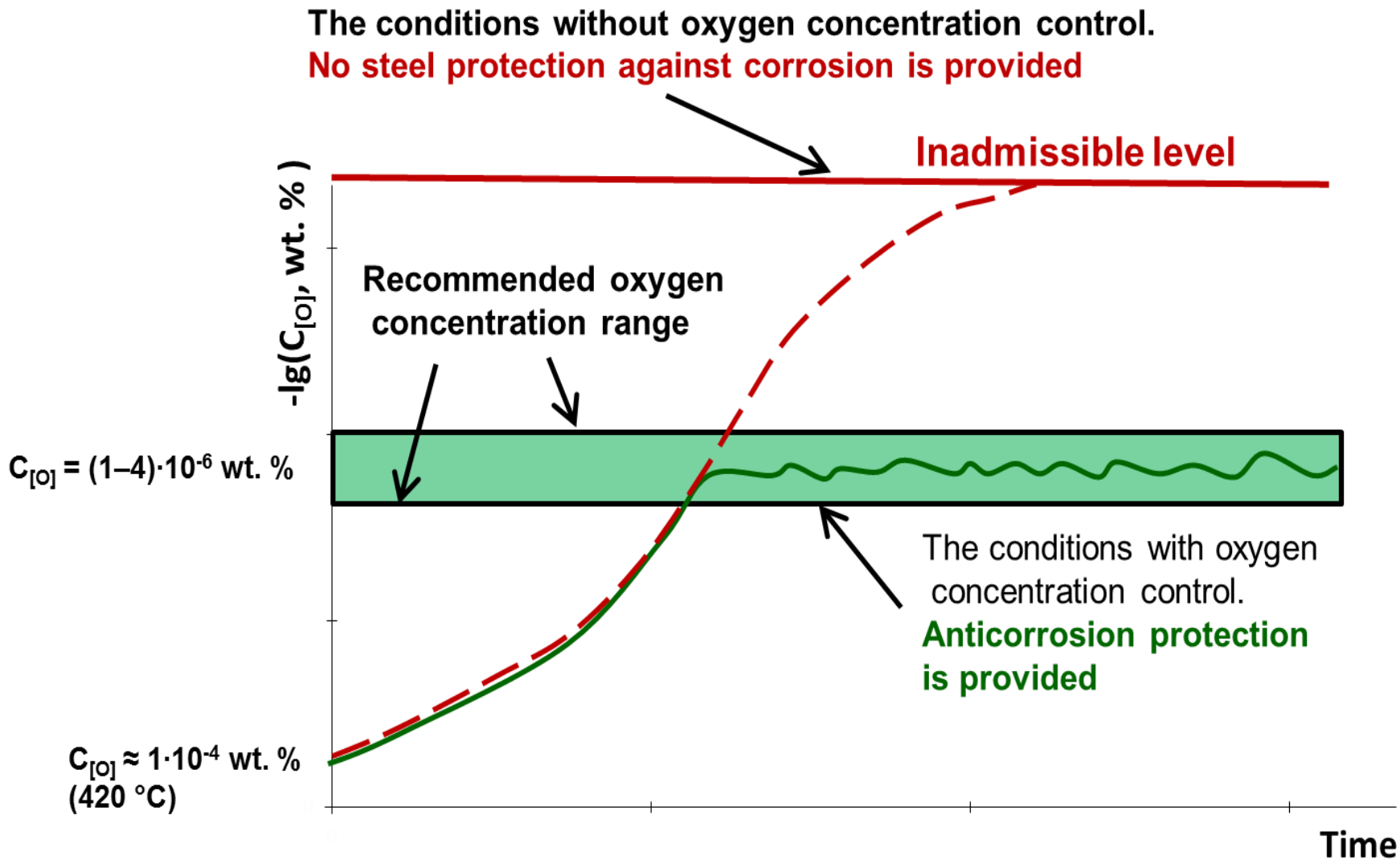

Solid-phase oxidant – granulated lead oxide

POCATOM

SSC RF – IPPE

Solid-phase oxidant (PbO)

The solid-phase method of control is based on dissolution of solid-phase oxide in interaction with coolant

$$\langle PbO \rangle \rightarrow \{Pb\} + [O]$$

< > - solid; { } – liquid; [ ] - dissolved

$$Sh = 8{,}7 \cdot 10^{-4} \cdot Re^{1.42} \cdot Sc^{0.83} \text{ (for Pb)}$$

$$K_p = Sh \cdot D/l \cdot Cs \cdot \rho \cdot 360,$$

Kp - dissolution rate coefficient, $g_{[O]}/(cm^2 \langle PbO \rangle \cdot h)$;
Sh - Sherwood criterion;
D – diffusion coefficient, m^2/s;
l – characteristic dimension, m;
Cs – oxygen solubility in lead;
ρ – lead density.

$$q = K_p \cdot (1-a) \cdot S,$$

q – capacity in oxygen, $g_{[O]}/h$;
a – oxygen TDA;
S – dissolution surface area, cm^2

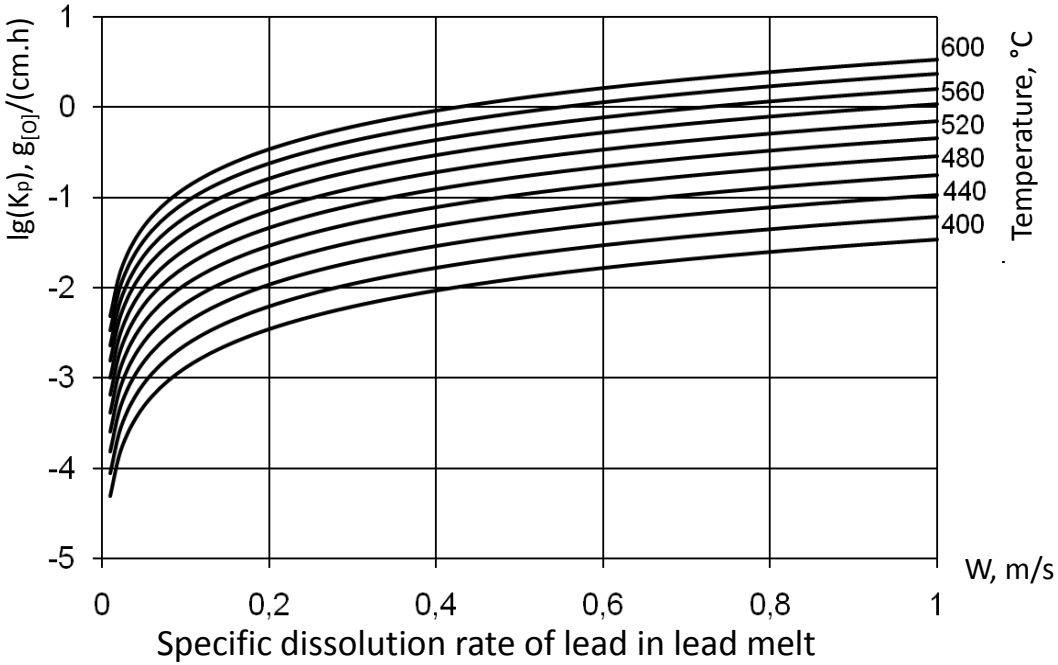

OXYGEN DISPENSERS (MASS TRANSFER APPARATUS) TO MAINTAIN OXYGEN CONDITIONS IN HEAVY LIQUID METAL COOLANT

POCATOM

SSC RF– IPPE

{Pb} + <PbO> → 2 {Pb} + [O]

< > – solid; { } – liquid; [ ] – dissolved

Solid-phase oxidizer:

A) Initial state;

B) at the end of its cycle

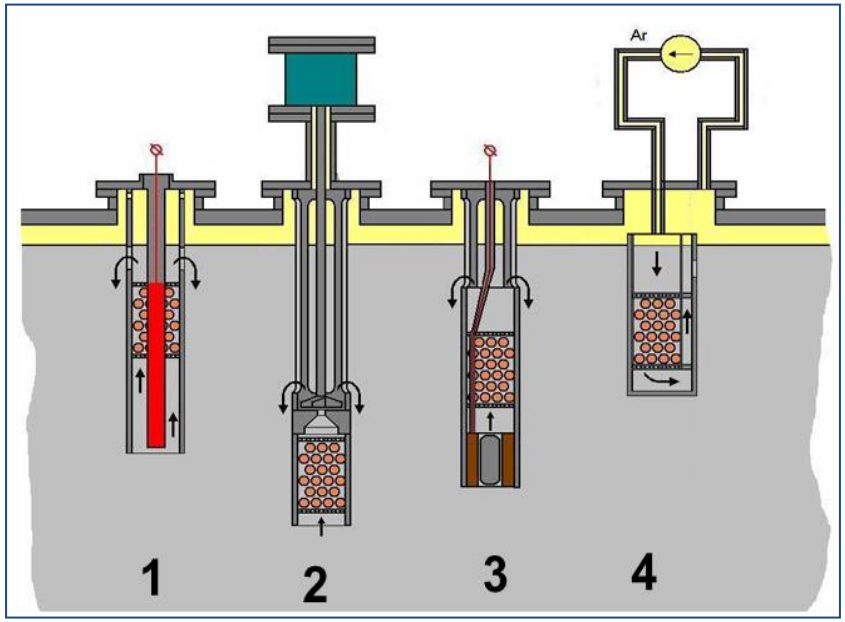

Mass transfer apparatus (MTA) types:

1. MTA with a built-in electric heater;
2. MTA with its own pump;
3. MTA with its own electromagnetic pump;
4. MTA of a gas lift type

Assumptions, which is accepted in the calculation technique

1. **Dissolution of oxide lead into the coolant is considered as physical dissolution of a solid body in liquid. A diffusion leading of the oxygen from a surface through a boundary layer limits the dissolution process.**
2. **A solubility of oxygen in the coolant is chose as a standard condition.**
3. **The relationship of a thermodynamic activity and concentration of dissolved oxygen in the coolant is determined by ratio:**

$$a_{[O]} = C/C_s$$

где: C – the concentration of dissolved oxygen in the coolant;

C_s – solubility of oxygen in the coolant.

4. **Granules PbO don't change its form during the dissolution process.**
5. **In a single cycle of the mass exchanger operation an influence of a change of the dimension granules to the other parameters is very insignificant.**
6. **A surface of granules in each point of reaction zone of the mass exchanger is equally accessible**

Calculation procedure of productivity

The main low of the solid state dissolution kinetics

$$\frac{dm}{S_p \cdot d\tau} = K \cdot (C_s - C)$$

Balance equation

$$m_{[O]_0} - m_{[O]} = V_{coolant} \cdot \rho_{coolant} \cdot (C_{[O]} - C_0)$$

With a glance the correlation

$$a_{[O]} = \frac{C}{C_s},$$

$$-\frac{dm_{[O]}}{d\tau} = K_p \cdot (1 - a_{[O]}) \cdot S_p$$

In differential species

$$dm_{[O]} = V_{coolant} \cdot \rho_{coolant} \cdot dC_{[O]}$$

$$A = (6/d) \cdot (1-\varepsilon)$$

$$S_p = A \cdot V_{MA}$$

$$dm_{[O]} = \varepsilon \cdot V_{MA} \cdot \rho_{coolant} \cdot Cs \cdot da_{[O]}$$

$$-dm_{[O]} = K_p \cdot (1 - a_{[O]}) \cdot A \cdot V_{MA} \cdot d\tau$$

$$V_{coolant} = \varepsilon \cdot V_{PE}$$

$$dC_{[O]} = Cs_{[O]} \cdot da_{[O]}$$

After separation of variables

$$-\frac{da_{[O]}}{(1 - a_{[O]})} = \frac{K_p}{\varepsilon \cdot \rho_{coolant} \cdot Cs} \cdot A \cdot d\tau$$

After integration

$$a_{[O]} = 1 - (1 - a_{[O]inlet}) \cdot \exp[-\frac{K_p \cdot A}{\varepsilon \cdot \rho_{coolant} \cdot Cs} \cdot \tau_c]$$

Productivity of mass exchanger

$$q = \rho_{coolant} \cdot Q_{coolant} \cdot Cs \cdot (a_{[O]outlet} - a_{[O]inlet})$$

Calculation technique of the change of granules dimension

Radius of granules in the mass exchanger with continuous flow rate of the coolant

$$r = r_0 - \frac{K_p \cdot (1 - a_{[O]in}) \cdot \Delta\tau}{\frac{\mu_O}{\mu_{PbO}} \cdot \rho_{PbO}}$$

(for granules, which is placed near an inlet)

$$r = r_0 - \frac{K_p \cdot (1 - a_{[O]out}) \cdot \Delta\tau}{\frac{\mu_O}{\mu_{PbO}} \cdot \rho_{PbO}}$$

(for granules, which is placed near an outlet)

r — medium radius of the granules;

$\Delta\tau$ – operation time;

$a_{[O]}$ — thermodynamic activity;

K_P — a coefficient of dissolution rate;

μ_O ,μ_{PbO} – molar mass of oxygen and lead oxide;

ρ_{PbO} – density of lead oxide.

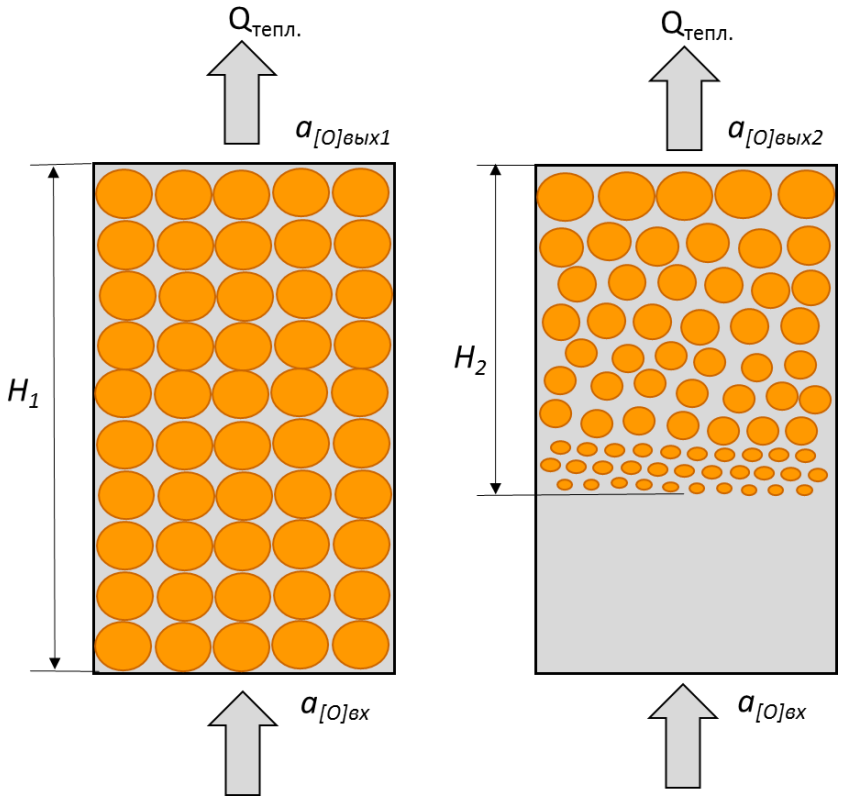

Start condition

Condition after the operation time Δτ

The calculation technique of the productivity change

1. Calculation of outlet thermodynamic activity in start condition
2. Calculation of mass exchanger productivity in start condition
3. Calculation of the change of dimension granules (inlet and outlet) after the time dτ (time step)
4. Calculation of outlet thermodynamic activity after the time dτ
5. Calculation of the mass exchanger productivity after the time dτ
6. Continue performing the iterative process until the performance value q < qmin will be reached

q_{min} – a minimum value of the mass exchanger productivity. It is supposed that the operation life of mass exchanger is finished when the specified value is achieved

Examples of calculation results

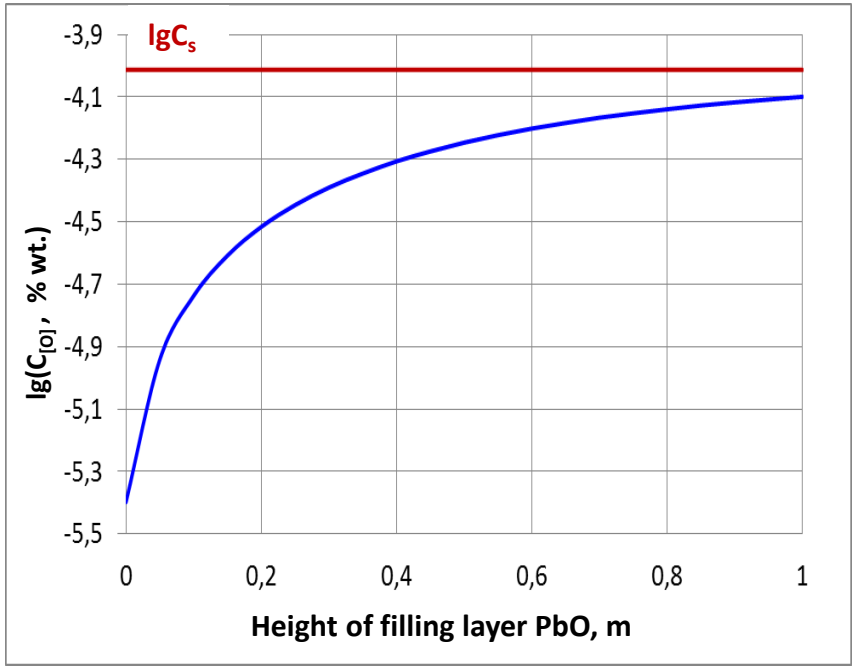

An example of a change of the oxygen concentration in the filling

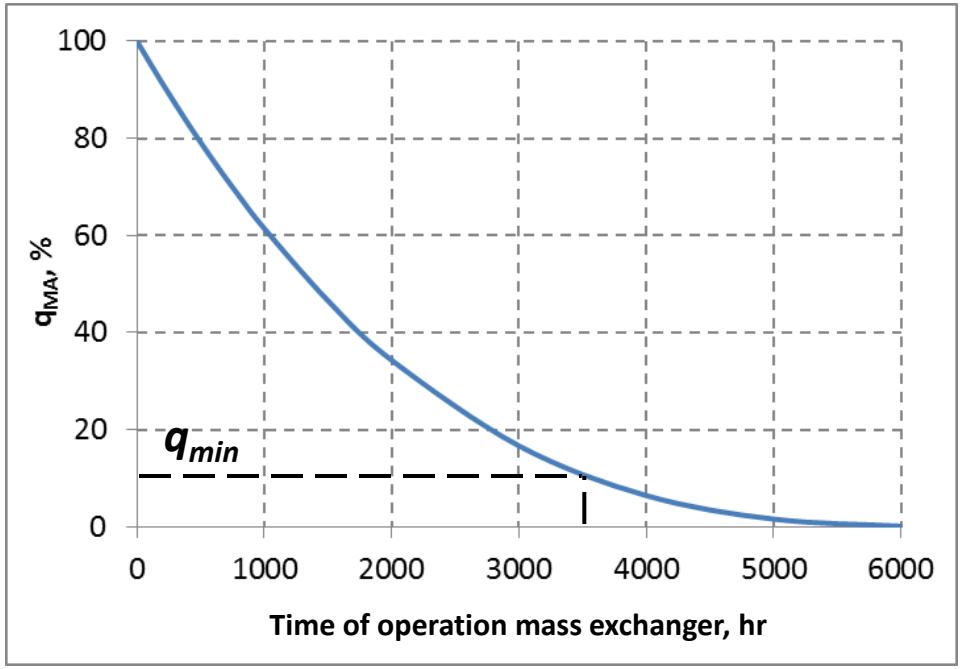

An example of the productivity change

Typical dependence of the mass exchanger resource on the intensity of oxygen consumption

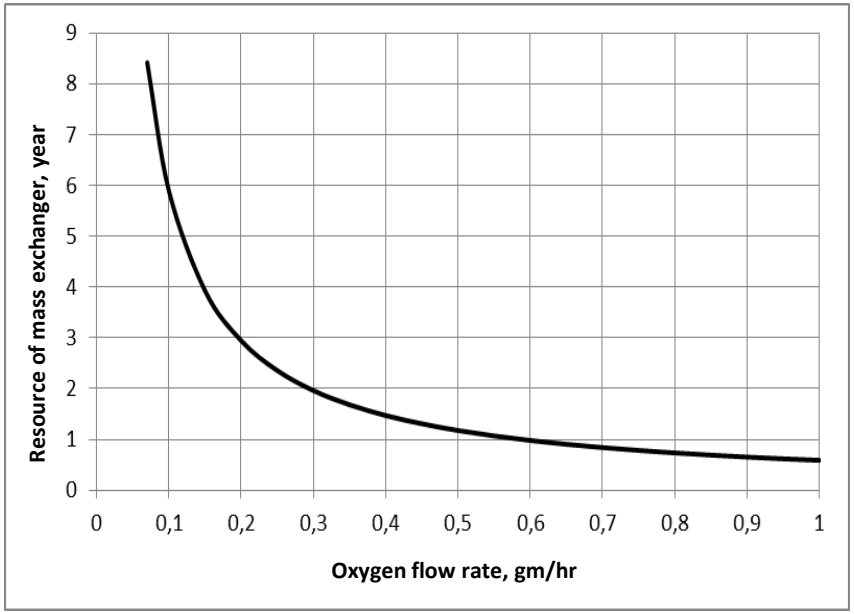

Dependence of the mass exchanger resource on the constant intensity of oxygen consumption by the circuit

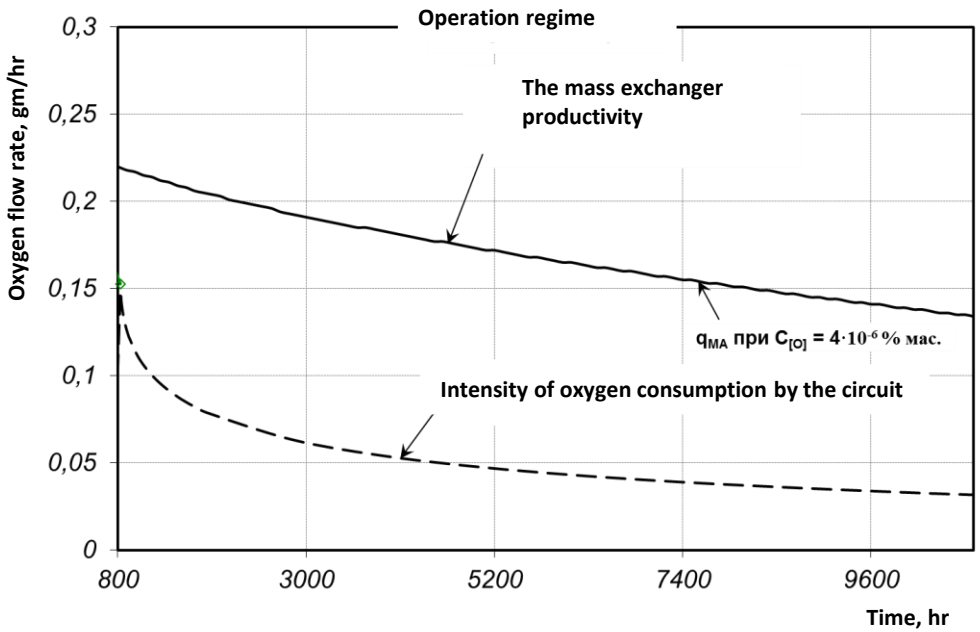

Typical change in performance of mass exchanger and intensity of oxygen consumption by the circuit during the operation

The resource of the mass exchanger and the rate of change in its performance depend significantly on the intensity of oxygen consumption by the circulation circuit

Conclusion

1. The productivity of mass exchanger changes during the operation on account of decrease of the dimension lead oxide granules.

2. Reducing of granules dimension is uneven in the filling layer: at the inlet to the filling, the rate of reduction of the granules is higher than at the outlet from it.

3. The criteria of the mass exchanger operation finish is minimum value of its productivity. It is supposed that the operation life of mass exchanger is finished when the specified value of minimum productivity is achieved.

4. The resource of the mass exchanger and the rate of change in its performance depend significantly on the intensity of oxygen consumption by the circulation circuit.

5. Create calculation technique allows to predict the change of the productivity mass exchanger during the operation.

РОСАТОМ

ГНЦ РФ – ФЭИ

THANK YOU
FOR
YOUR ATTENTION!

STATE SCIENTIFIC CENTER OF RUSSIAN FEDERATION -
INSTITUTE OF PHYSICS AND POWER ENGINEERING
named after A.I. Leypunsky
SSC RF-IPPE DIVISION OF STATE CORPORATION "ROSATOM"

«Study on kinetics of lead and bismuth oxides reduction by hydrogen for applying in HLMC technology»

Authors: **I.I. Ivanov**, V.M. Shelemet'ev, R.Sh. Askhadullin, D.A. Skobeev

SSC RF-IPPE, Obninsk

E-mail: iivanov@ippe.ru

Information on the kinetics of hydrogen reduction of lead and bismuth oxides is necessary for the optimization of the following processes:

- hydrogen purification of circulation circuits with heavy liquid-metal coolants from slag deposits based on lead oxides;

- removal of hydrogen remained after hydrogen regeneration, as well as tritium from the protective gas of the primary circuit.

Hydrogen purification of circuits with HLMC

In the process of operation of circuits with HLMC due to the interaction of the coolant with air, slag deposits are formed, which impair heat exchange and coolant circulation.

“Hydrogen-noble gas-water” vapor mixtures are introduced into the coolant flow and protective gas to purify the contours from the slag deposits. Cleaning is achieved due to two factors:

- mechanical (crushing) effects of two-phase flow;

- chemical interaction of hydrogen with lead oxide, during which lead oxide is reduced to metal, and the resulting water vapor is separated and condensed in the cold zone of the gas loop.

Cover gas purification from hydrogen and tritium

The hydrogen remained after the hydrogen regeneration must be removed from the gas circuit, as well as the tritium that poses a great danger.

For this purpose, a special device (afterburner) is designed, the main element of which is a heated chamber filled with a reagent (lead or bismuth oxide). Ufter hydrogen and tritium interaction with oxides, water (reaction product) condenses in the cold zone of the gas circuit, where it is drained for disposal.

Considering reactions:

$$Bi_2O_3 + 3H_2 = 2Bi + 3H_2O \quad (1)$$

$$PbO + H_2 = Pb + H_2O \quad (2)$$

Main characteristics of the kinetics of reduction:

- Kinetic equation (the dependence of the degree of reduction or reduction rate on time, at constant values of other parameters);
- Dependence of the reaction rate on temperature;
- Dependence of the reaction rate on the partial pressure of hydrogen.

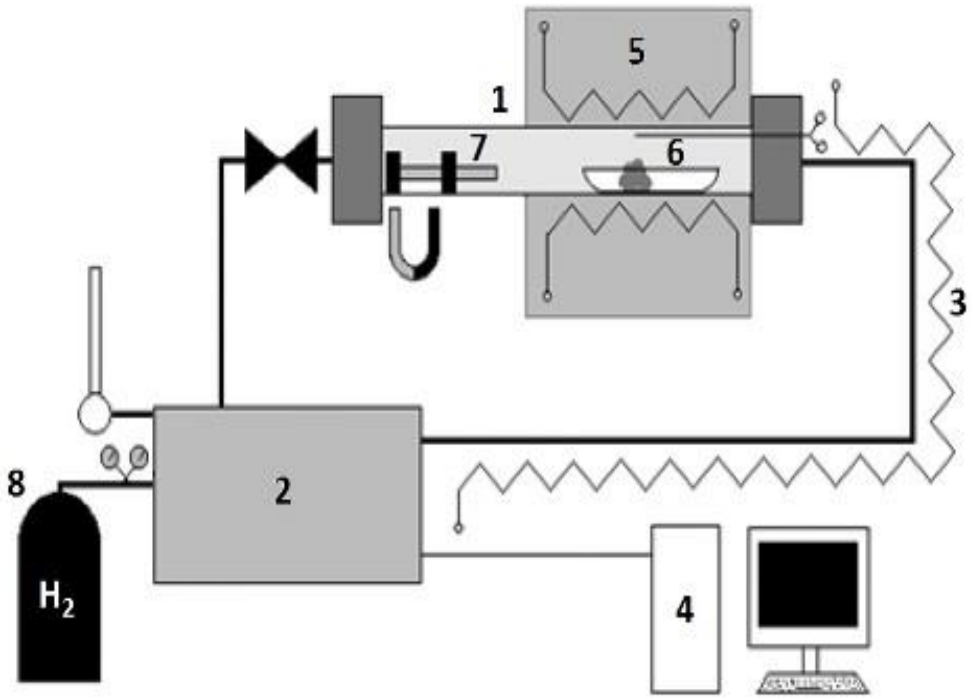

Fig. 1. Scheme of the installation for the study of the reduction kinetics of oxides by hydrogen. 1-reaction chamber; 2-chromatograph; 3-heated gas line; 4-signal recording unit; 5-oven; 6-boat with sample and thermocouple; 7-quartz piston; 8-cylinder with hydrogen.

Method of data processing by affine time transformation

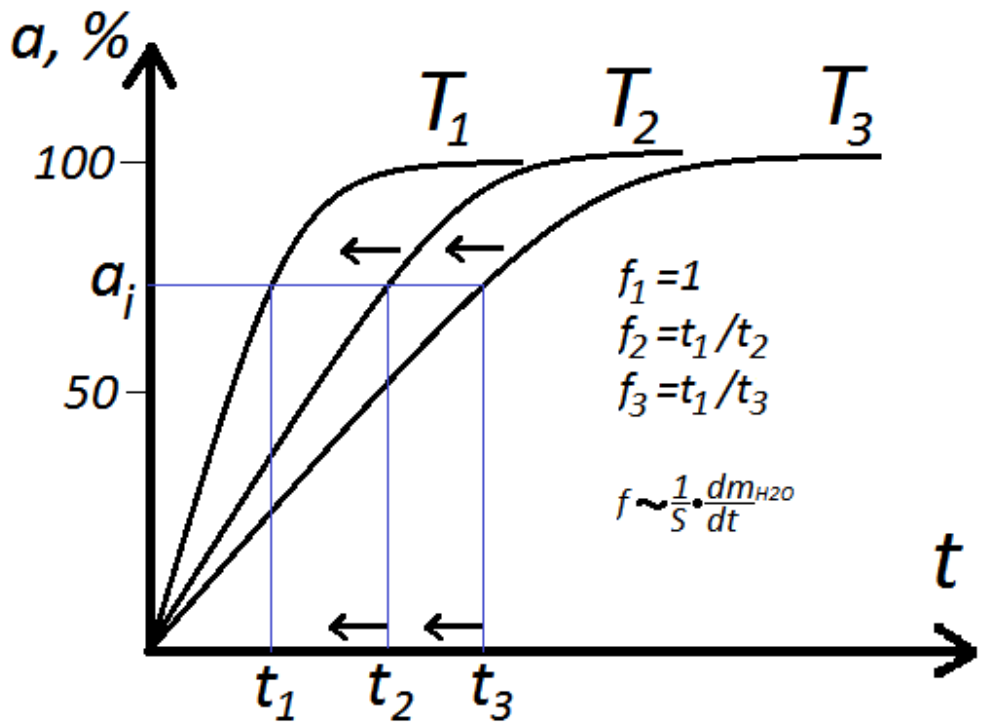

Fig. 2. Method of affine time transformation

This method consists in changing of time scale for every kinetic curve to combine all curves together. For every curve *k* and for every value of degree of reduction a_i coefficient of affine time transformation $f_{i,\,k}$ can be calculated. Also middle value of affine time transformation coefficient f_k can be calculated for every curve. This middle value of coefficient *f* was used in this work for calculations. Coefficient f_k is directly proportional to specific reaction rate (rate per unit of oxide powder surface).

Kinetics of reduction of bismuth oxide by hydrogen

$$\alpha(t) = 100 \cdot \frac{m_{Me_xO_y}(t)}{m^0_{Me_xO_y}} \quad (1)$$

$$\alpha(t) = 100 \cdot (1 - \exp[-k \cdot t]) \quad (2)$$

$$k = f(T, c_{H_2}) \quad (3)$$

Value *k* is directly proportional to specific reaction rate, which is total reaction rate divided by value of sample free surface.

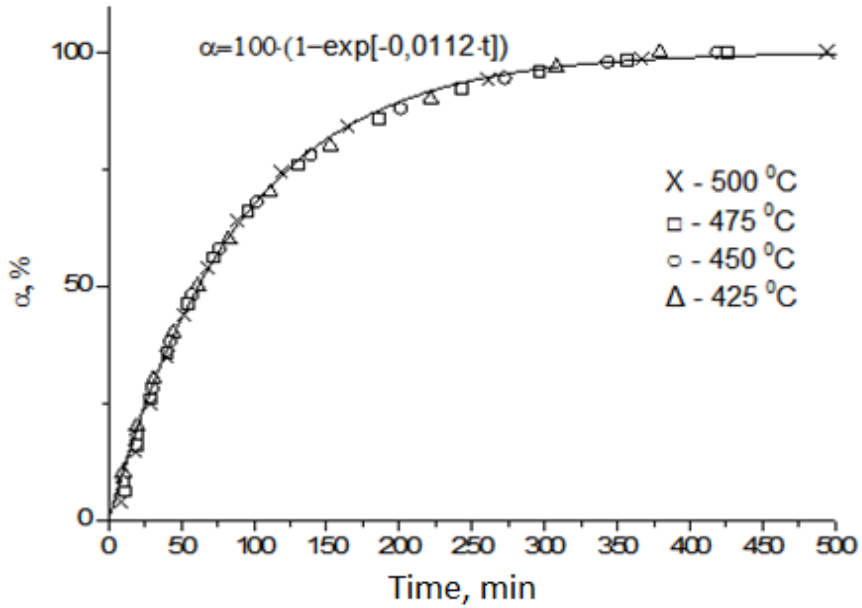

Fig. 3. Dependence of the degree of bismuth oxide reduction on time, obtained at temperatures of 425, 450, 475 and 500 °C and combined with an affine time transformation. A "fat" line is an approximation of the obtained dependences by an exponential function.

Kinetics of reduction of bismuth oxide by hydrogen

$$k = b \cdot \exp(\frac{-92800}{R \cdot T}) \quad (4)$$

$$b = f(c_{H_2}) \quad (5)$$

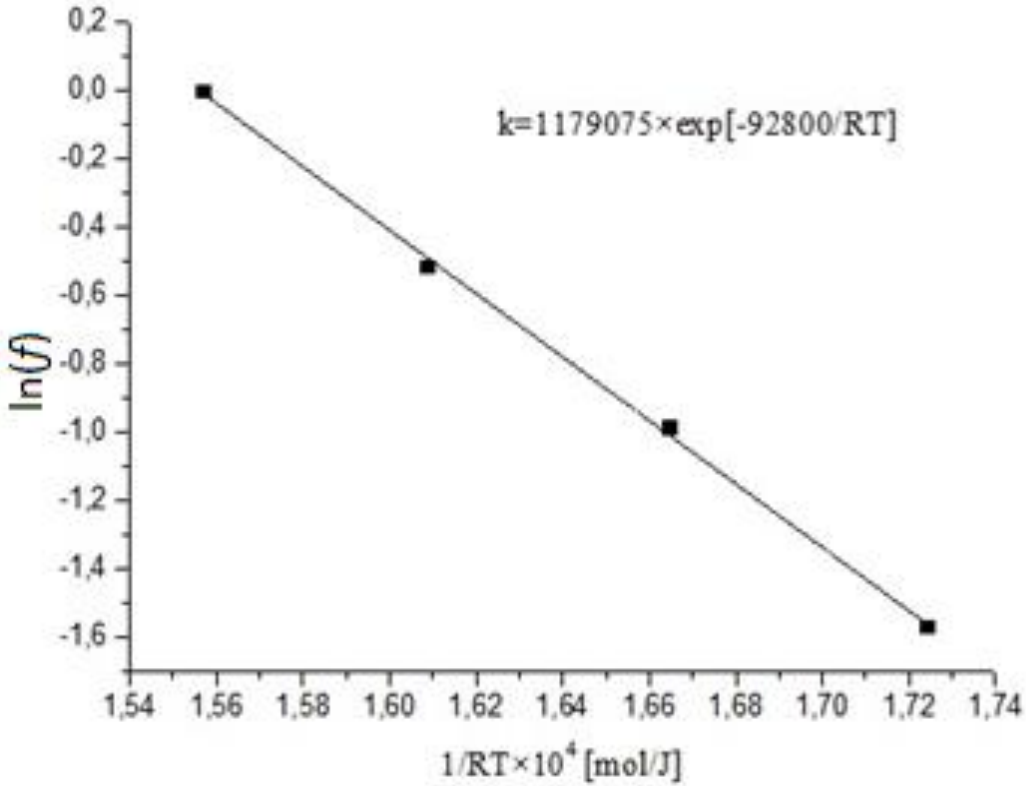

Fig. 4. Dependence of ln (f) on 1/RT for the reduction of bismuth oxide powder by hydrogen. T - in Kelvins

Kinetics of reduction of bismuth oxide by hydrogen

$$b = d \cdot c_{H_2} \tag{6}$$

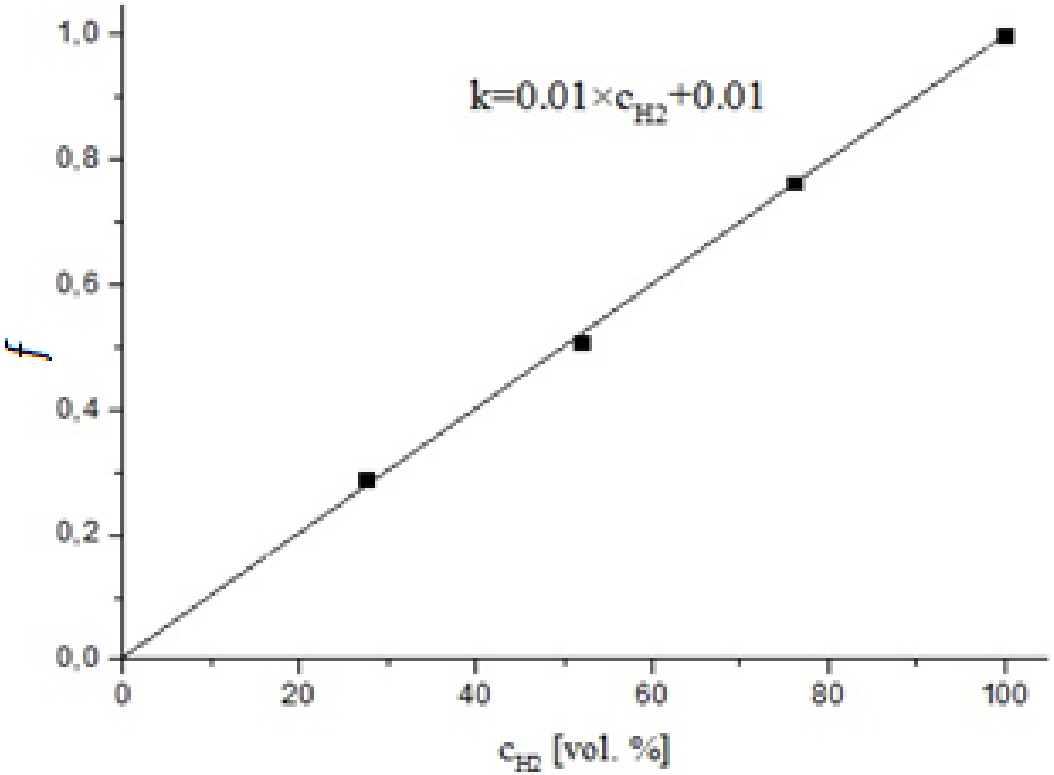

Fig. 5. Dependence of the coefficient of the affine time transformation *f* on the volume concentration of hydrogen (in %) at a reduction temperature of bismuth oxide of 500 °C.

Kinetics of reduction of lead oxide by hydrogen

$$\alpha(t) = 100 \cdot [1 - \exp(-k \cdot t)] \quad (7)$$

$$\frac{d\alpha}{dt} = 100 \cdot k \cdot \exp(-k \cdot t) \quad (8)$$

$$\frac{d\alpha}{dt} = k \cdot \big(100 - \alpha(t)\big) = k \cdot 100 \left(1 - \frac{1}{m_{PbO}^{0}} \cdot \frac{dm_{PbO}}{dt}\right) =$$

$$= k \cdot 100 \left(1 - \frac{100 M_{H_2O}}{3 m_{PbO}^{0} \cdot M_{PbO}} \cdot \frac{dm_{H_2O}}{dt}\right) \quad (9)$$

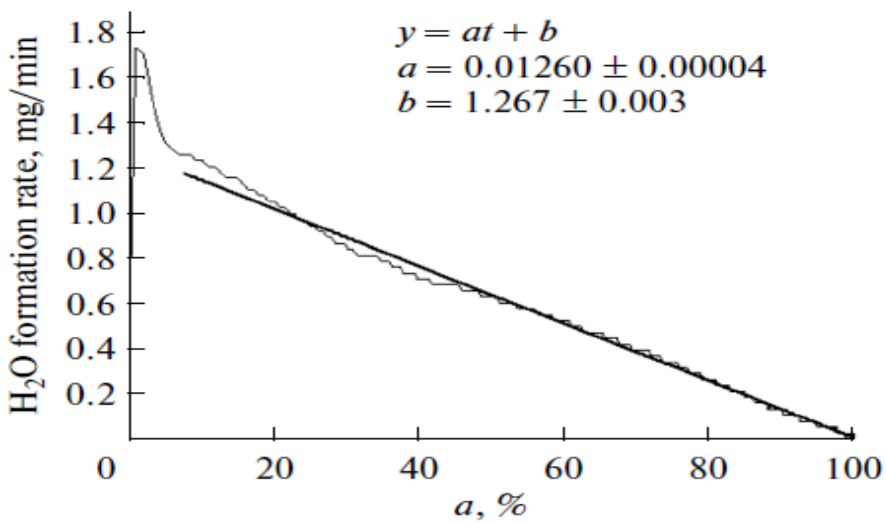

Fig. 6. Dependence of the rate of water formation on the degree of reduction at 500 °C.

Kinetics of reduction of lead oxide by hydrogen

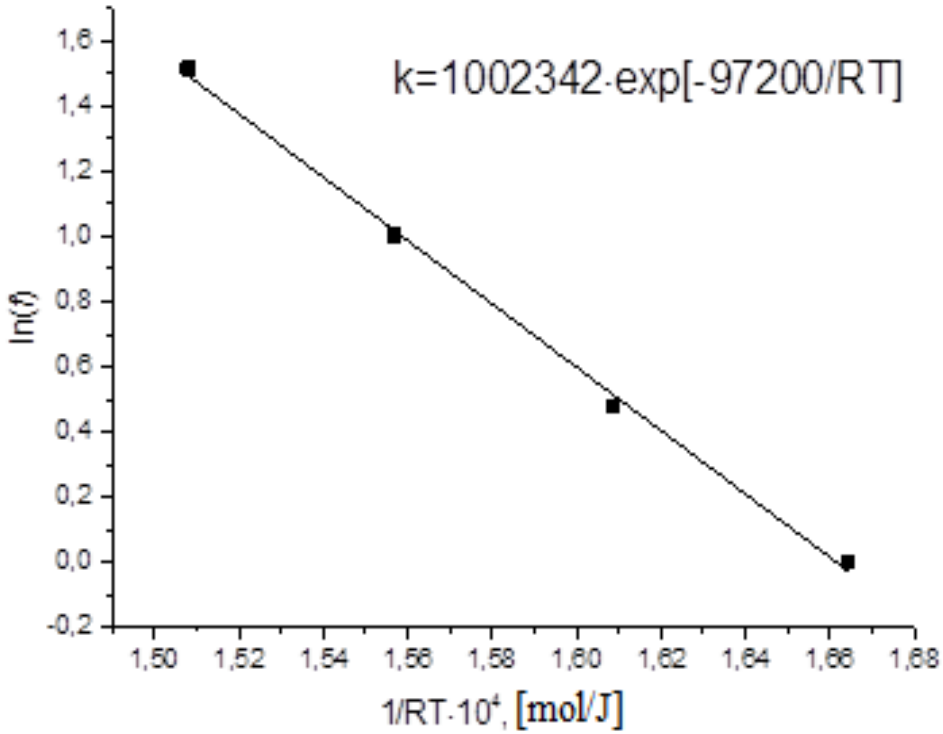

Fig. 7. Dependence of ln (*f*) on 1/RT for the reduction of lead oxide powder by hydrogen. T – in Kelvins

The main features of the hydrogen reduction of lead and bismuth oxides

By combination of equations 2, 4 and 6, general kinetics equation can be obtained:

$$\alpha\left(t, T, c_{H_2}\right) = 100 \cdot (1 - \exp\left[-d \cdot c_{H_2} \cdot \exp\left[\frac{-E_a}{R \cdot T}\right] \cdot t\right]),$$

where d is the constant for a given oxide sample, which depends on structural defectiveness and value of its surface, E_a is the activation energy equal to 92.8 kJ/mol for bismuth oxide and 97.2 kJ/mol for lead oxide. This allows to give the following recommendations for carrying out reduction processes:

- It is advisable to provide the reduction at a temperature close to the maximum permissible for a given technological operation (for example, determined by the upper temperature limit of the corrosion resistance of steel in the case of hydrogen regeneration of the circuit.
- For regeneration, it is necessary to use a gas mixture with the maximum permissible hydrogen concentration.

Thank you for attantion!

Effect of the design of the reference electrode on the metrological characteristics of the solid electrolyte oxygen sensor

Shelemet'ev Vasiliy Mikhailovich

SSC RF - IPPE
Phone: 8 (48439) 9-42-77
E-mail: vshelemetev@ippe.ru

Obninsk 2018

High-temperature sensors for oxygen and hydrogen control in gaseous and liquid media

ROSATOM

ГНЦ РФ-ФЭИ

Sensors

Nuclear industry

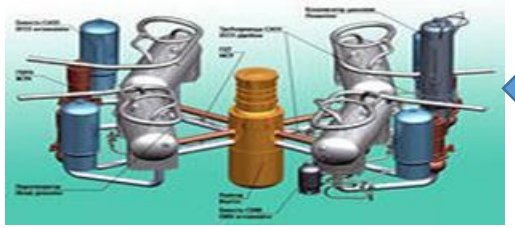

Liquid metal circulation circuites of NPP

Gas circuites of NPP

NPP containment

Housing and utilities

Chemical industry

Manufactures associated with the production, use, recycling or storage of flammable gases (hydrogen, oxygen, methane, propane, etc.) and vapors of flammable liquids (alcohol, etc.)

Special warehouses and storage facilities

Oil- and gas recycling

Oxygen and hydrogen control sensors are placed on research stands (Russia, Italy), at nuclear power plants (Russia, China, India, Iran).

Design and operation principle of solid electrolyte oxygen sensor in gases and HLMC

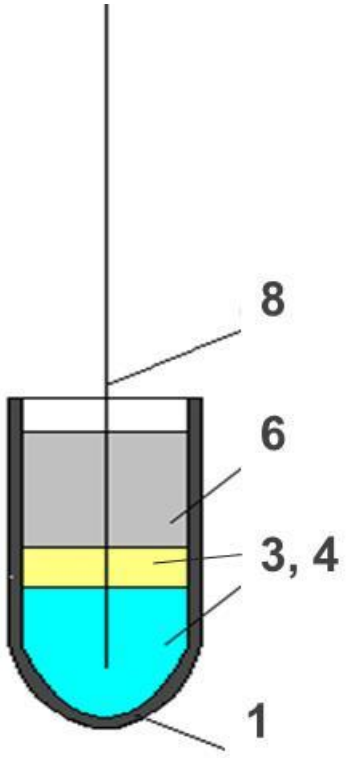

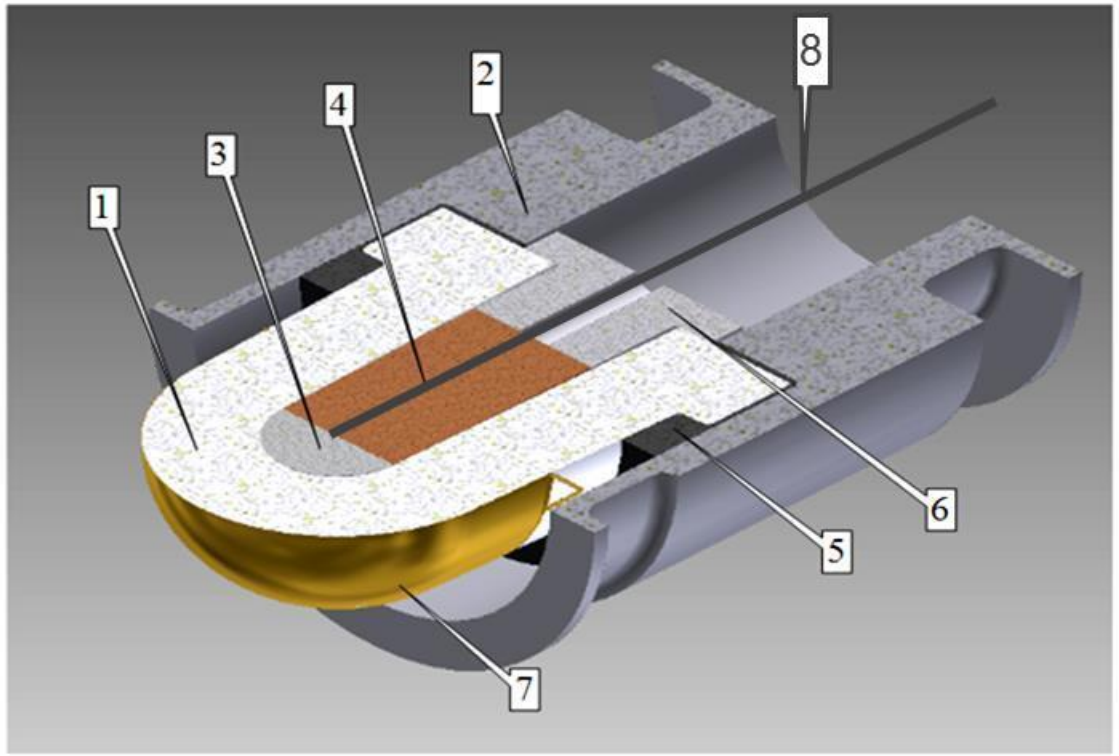

1 - ceramic sensor element; 2 - case, ferritic-martensitic steel;
3 - reference electrode, metal (Bi); 4 - oxygen source for the reference electrode, - metal oxide (Bi2O3);
5 - high-temperature sealant; 6 - sealing stopper; 7 - measuring electrode; 8 – electrical lead

$$E = \frac{R \cdot T}{n \cdot F} \cdot \ln\left(\frac{P_{O_2}}{P_{O_{2\,ref}}}\right)$$

$Po_{2\,ref}$, Po_2 – the partial pressure of oxygen in the reference electrode and the medium to be analyzed, respectively

Comparative characteristics of solid electrolyte oxygen sensors in gases and ТЖМТ with reference electrode Bi- Bi_2O_3 and In-In_2O_3 with Mo potential-absorbers

Experience in the operation of sensors with the reference electrode Bi- Bi_2O_3 and In-In_2O_3 with Mo electrical lead demonstrated significant differences in the metrological characteristics of the sensors:

- A more pronounced (several times) drift in the readings of the sensor with the reference electrode Bi-Bi_2O_3;
- More pronounced polarizability of the reference electrode in the case of using the Bi-Bi_2O_3 system;
- A sharp change in the signal level, with constant parameters of the analyzed medium (composition, temperature, pressure), for example, when vibrating;
- The discrepancy between the experimentally determined difference in the sensor readings with a theoretical value determined from the thermodynamic calculation by up to several tens of mV.

During the research, it was suggested that the reason for the above-mentioned effects is the oxidation of the Mo electrical lead when interacting with the oxygen-saturated Bi.

Thermodynamics of the system In-In_2O_3-Mo и Bi- Bi_2O_3 -Mo

Within the framework of theoretical justification of the assumption, the possibility of oxidation of Mo with In oxide to the lowest oxide of $MoO2$ by the reaction:

$$2In_2O_3 + 3Mo = 3MoO_2 + 2In$$

and oxidation of Mo with Bi oxide to a higher oxide$MoO_2$by the reaction:

$$Bi_2O_3 + Mo = MoO_3 + 2Bi$$

The results of the thermodynamic calculation are given in the table:

Temperature, °C	$\Delta G_{In_2O_3}$, J/mol	ΔG_{MoO_2}, J/mol	$\Delta G_{(2)}$, J/mol	$\Delta G_{Bi_2O_3}$, J/mol	ΔG_{MoO_3}, J/mol	$\Delta G_{(3)}$, J/mol
400	-702484	-459947	25126	-392849	-583683	-190834
500	-671735	-443327	13488	-363614	-559092	-195478
530	-662511	-438341	9997	-354843	-551714	-196871

It can be seen from the table that the oxidation of Mo by In oxide does not occur spontaneously, hence an oxide layer is not formed on the Mo surface.

In contrast, Mo is oxidized by Bi oxide to higher MoO_3 oxide. This means the possibility of forming molybdenum oxides with a lower valence, as well as mixed oxides of molybdenum and bismuth.

The composition of the oxide film at the interface Bi- Bi_2O_3 -Mo

An extensive study [1], devoted to the study of the phase composition of the system Bi-Mo-O, revealed at a temperature 500 °C (aging of samples 960 hours) the existence of four different oxides containing molybdenum: MoO_2, Bi_2MoO_6, $Bi_2Mo_3O_{12}$. Also, according to the phase diagram Bi_2O_3 -MoO_3 [2] there are oxides $Bi_6Mo_2O_{15}$, Bi_6MoO_{12} and $Bi_{14}MoO_{24}$.

Other mixed oxides of Mo and Bi that can form part of the oxide film at the Bi-Mo interface can also be determined from the phase diagram of the system MoO_3-Bi_2O_3.

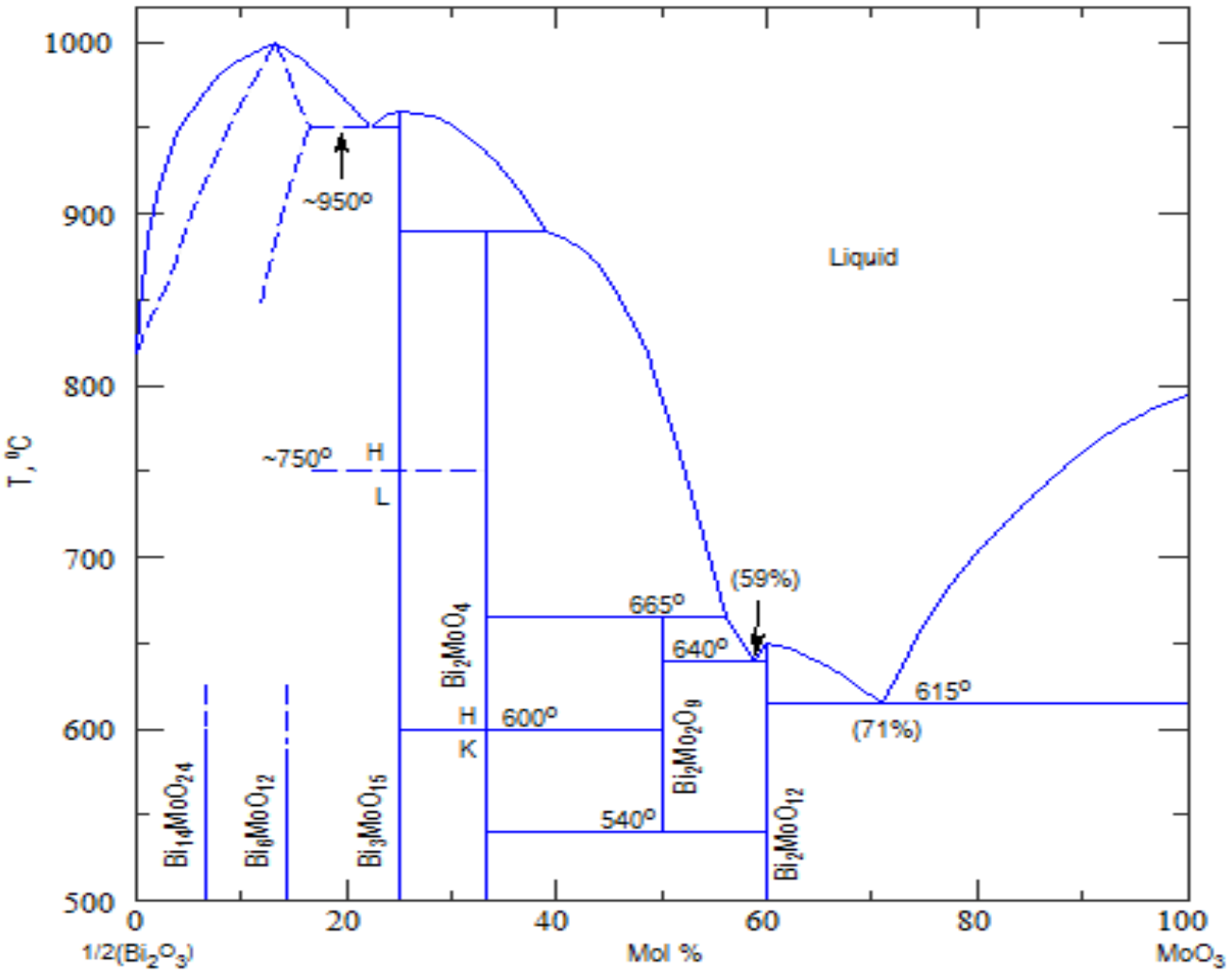

1. Aiswarya P.M., Ganesan R., Rajamadhavan R., Gnanasekaran T. Partial phase diagram of MoO3 rich section of the ternary Bi-Mo-O system // Journal of Alloys and Compounds, – 2018. – Vol. 745. – P. 744-752.
2. Egashira M., Matsuo K., Kagawa S., Seiyama T., Journal of catalysis, – 1979. – Vol. 58. – P. 409-418.

Experimental substantiation of the influence of the oxide layer on the surface of the Mo electrical lead on the metrological characteristics of the sensor

A sensor with a sensor reference electrode Bi- Bi_2O_3 and two electrical leads: Bi_2O_3 и Mo, The results are shown in the figure.

A clear difference in the readings obtained from different electrical leads is evident: pronounced drift of readings, jumps of EMF, significant discrepancy of readings (up to several tens of mV) in the case of the Mo electrical lead. A similar difference appeared in the case of the system In-In_2O_3-Mo.

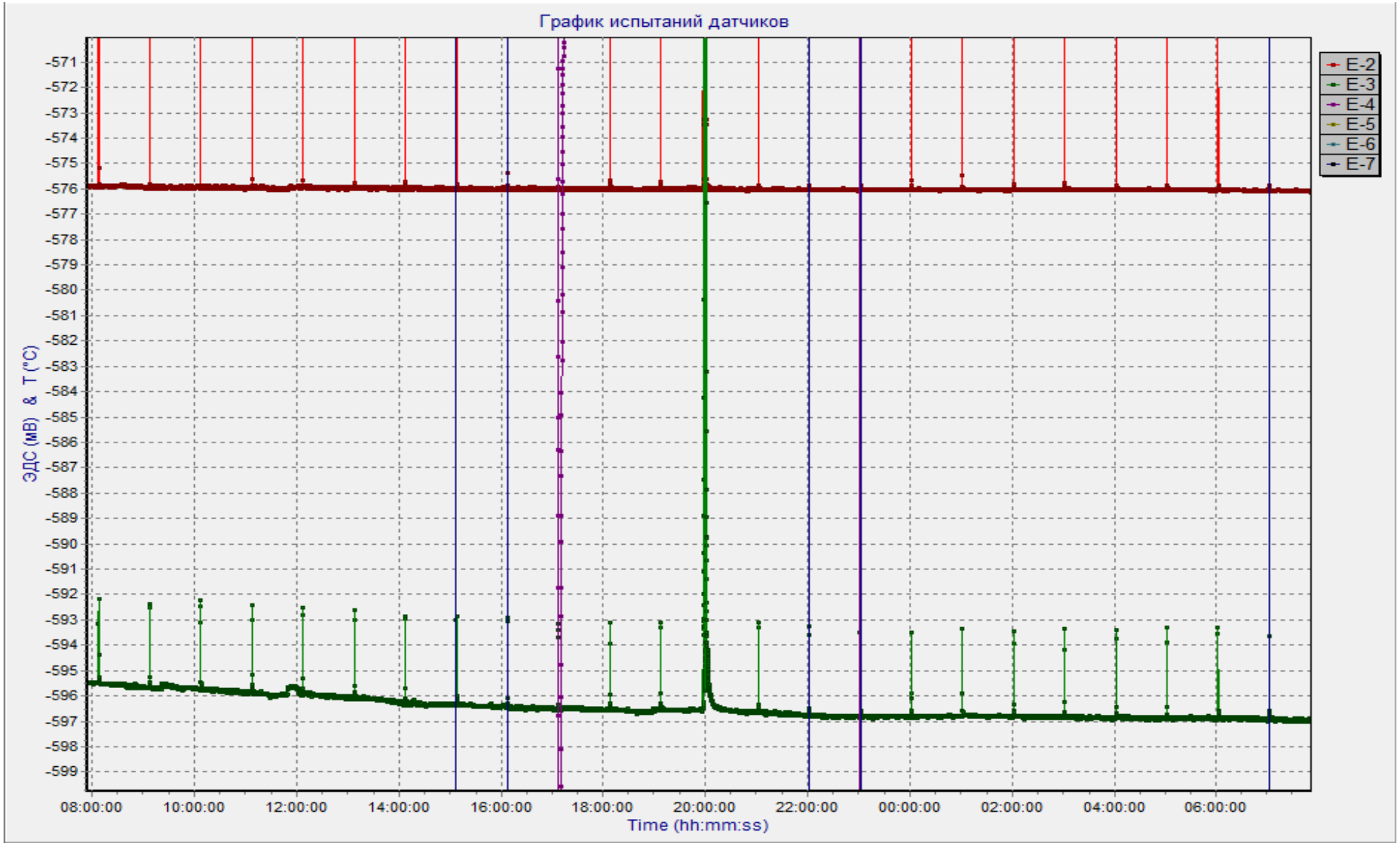

The main reasons for the instability of the sensor reading based on the system $Bi-Bi_2O_3-Mo$

- Partially ionic conductivity of the oxide layer on Mo, contributing to the total value of the EMF of the sensor;
- The change in the phase composition of the oxide layer over time, leading to a change in the contribution to the EMF of the sensor and, as a consequence, to the drift of the sensor signal;
- Periodic peeling of the growing oxide layer (in particular as a result of mechanical action on the sensor), leading to a sharp change in the EMF of the sensor;

Experimental substantiation of the influence of the oxide layer on the surface of the electrical lead on the metrological characteristics of the sensor

Similar instability of the readings was obtained using a sensor-based system Bi – Bi_2O_3 –W.

According to the literature data, W is often used as electrical lead of sensors with a reference electrode Bi– Bi_2O_3.

Change of EMF and internal resistance of solid electrolyte oxygen sensor in gases with reference electrode Bi/ Bi_2O_3 and tungsten electrical lead with short-term vibration action. Peak heights are directly proportional to the value of the internal resistance of the sensor.

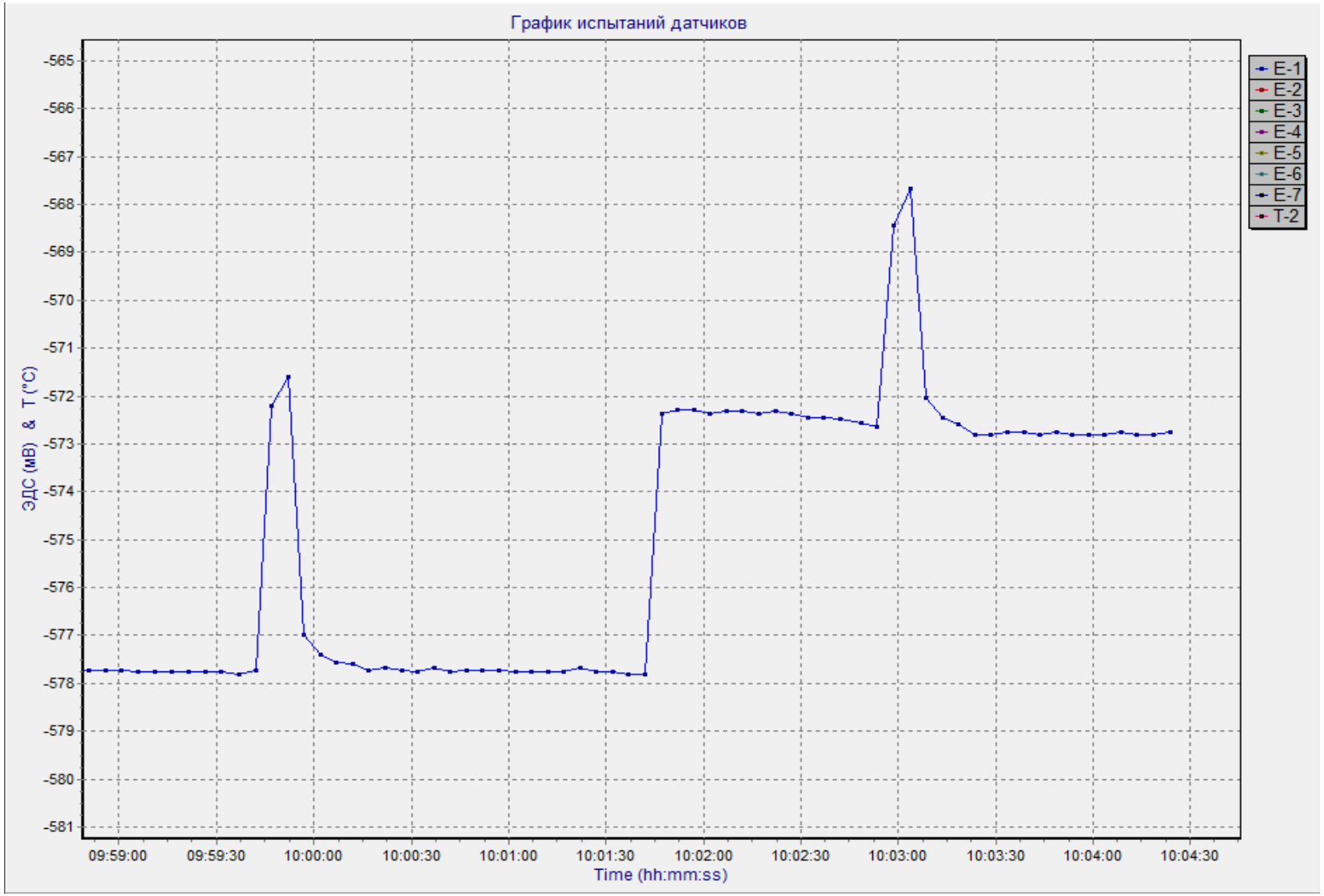

Thermodynamics of the system Bi-Bi_2O_3

For successful interpretation of the sensor readings, it is important to know the temperature dependence of the standard Gibbs energy of the reaction (the formation reaction of α-Bi_2O_3):

$$4Bi + 3O_2 = 2Bi_2O_3.$$

This dependence was obtained earlier in a number of works by the method of measuring EMF using a solid electrolyte based on zirconium dioxide, but in all cases, the electrical leads from materials whose chemical interaction with bismuth and its oxide have no exact data were immersed to measure the EMF in liquid bismuth. Therefore, the dependence of the standard Gibbs energy of the reaction on temperature was determined using an electrochemical cell structurally executed as a conventional solid-electrolyte oxygen sensor in a gas based system Bi-$Bi_2O_3$with electrical lead from Bi_2O_3.

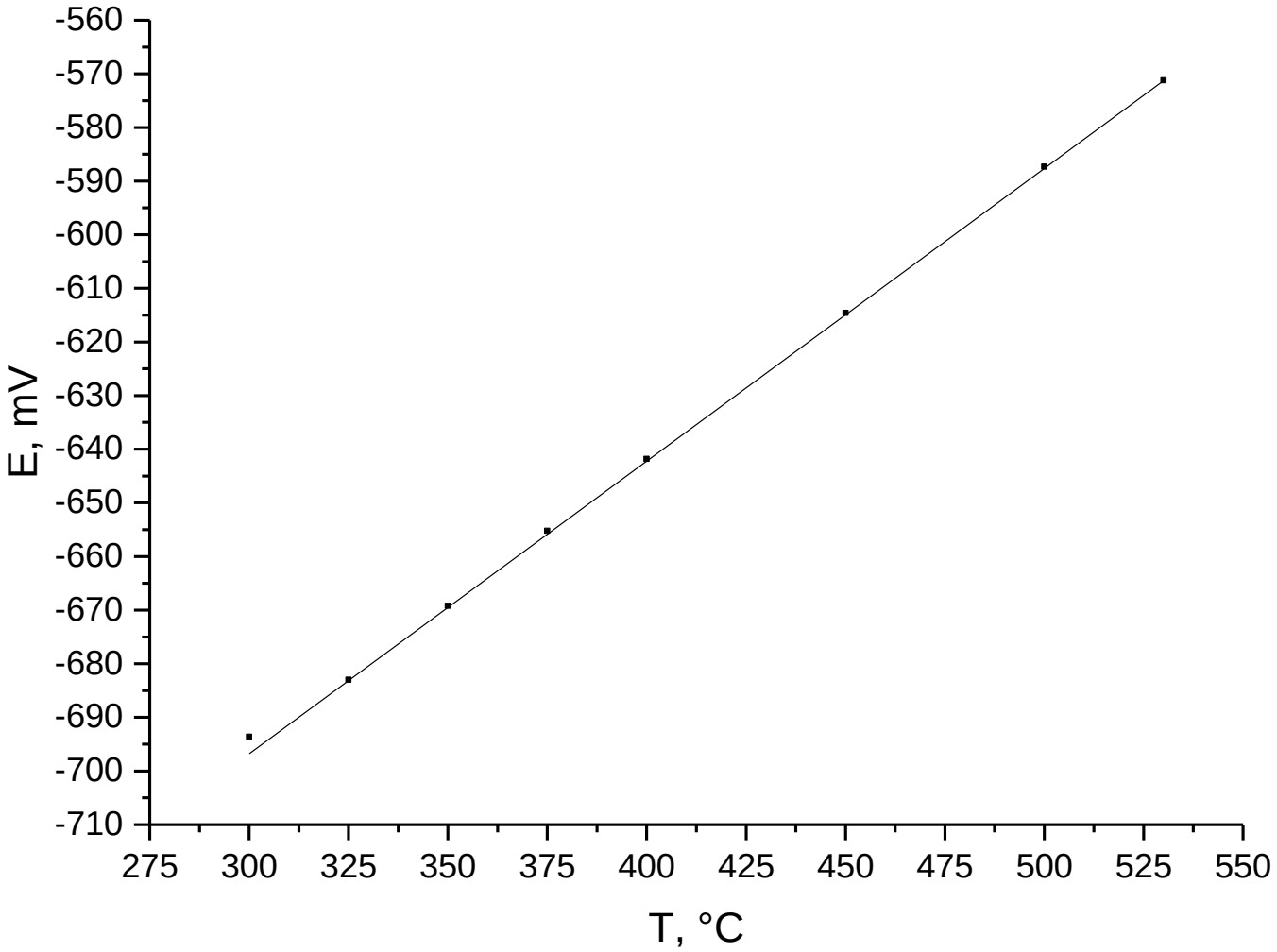

Dependence of the EMF of the sensor on the basis of the system Bi-Bi_2O_3 with electrical lead based on Bi_2O_3 on temperature

Thermodynamics of the system Bi-Bi_2O_3

The resulting expression for the dependence of the standard Gibbs energy (kJ / mol) of the reaction on temperature:

$$\Delta G^0_{Bi_2O_3} = -584.032 \pm 0.426 + (0.2961 \pm 0{,}006) \cdot T$$

The temperature dependence of the standard Gibbs energy (kJ/mol) of α- Bi_2O_3 formation according to the data of different authors:

Reference	Equation	Temperature range, K
Jacob et al. 2016	−584.235 + 0.28928·T	800–1002
Aspiala et al. 2014	−591.511 + 0.2934·T	572–988
Ganesan et al. 2003	−583.40 + 0.2938·T	572–988
Kulicov , 1986	−591.885+0.29259·T	544.5-1090
Schaefer et al. 1984	−581.994 + 0.2928·T	740–976
Fitzner et al. 1980	−605.283 + 0.31442·T	951–997
Ramana Rao et al. 1979	−629.608 + 0.3345·T	773–978
Isecke et al. 1979	−583.592 + 0.2939·T	823–980
Mehrotra et al. 1976	−600.900 + 0.3152·T	885–991

The obtained expression correlates with the data obtained recently with good accuracy.

Thermodynamics of the system $Bi\text{-}Bi_2O_3$

Based on the results of the analysis of the experimental conditions, it was concluded: $\Delta G^0_{Bi_2O_3} = -584.032 \pm 0.426 + (0.2961 \pm 0{,}006) \cdot T$

The temperature dependence of the standard Gibbs energy (kJ/mol) of formation α-Bi_2O_3 according to different authors:

Reference	Equation	Temperature range, K	Type of solid electrolyte	Reference electrode	Electrical lead of reference electrode
Jacob et al. 2016	−584.235 + 0.28928·T	800–1002	ZrO_2-Y_2O_3	Pt, O_2	Os
Aspiala et al. 2014	−591.511 + 0.2934·T	572–988	ZrO_2-Y_2O_3	Pt, O_2	Cr_2O_3
Ganesan et al. 2003	−583.40 + 0.2938·T	572–988	ZrO_2-CaO	Pt, O_2	W
Kulicov , 1986	-591.885+0.29259T	544.5-1090	?	?	?
Schaefer et al. 1984	−581.994 + 0.2928T	740–976	ZrO_2-CaO	Cu, Cu_2O	W
Fitzner et al. 1980	−605.283 + 0.31442T	951–997	?	Ni, NiO	?
Ramana Rao et al. 1979	−629.608 + 0.3345·T	773–978		Fe, FeO	?
Isecke et al. 1979	−583.592 + 0.2939T	823–980	ZrO_2-CaO	Pt, air	?
Mehrotra et al. 1976	−600.900 + 0.3152T	885–991	?	?	?

The obtained expression correlates with the data obtained recently with good accuracy.

Based on the available data, it can be concluded that the best convergence takes place in works where the system Pt, O_2 and Pt, air, was used as the reference electrode, as in the current work, since in this case the error associated with the inaccuracy of temperature measurement is minimal.

Between the material of electrical lead and the convergence of the data of different authors, there is no single-valued connection, probably because of the short duration of the experiments, during which the surfaces of electrical lead did not have time to oxidize.

Thermodynamics of the system Pb-PbO

Gibbs energy was also determined for the lead oxide formation reaction:

$Pb + 0.5O_2 = PbO.$

A sensor based on the Pb-PbO system with a PbO-based electrical lead was used for the experiment.

The resulting equation has the following form:

$$\Delta G^0_{PbO} = -218434 \pm 439 + (98{,}8 \pm 0{,}6) \cdot T$$

The equation is in good agreement with the data of other authors.

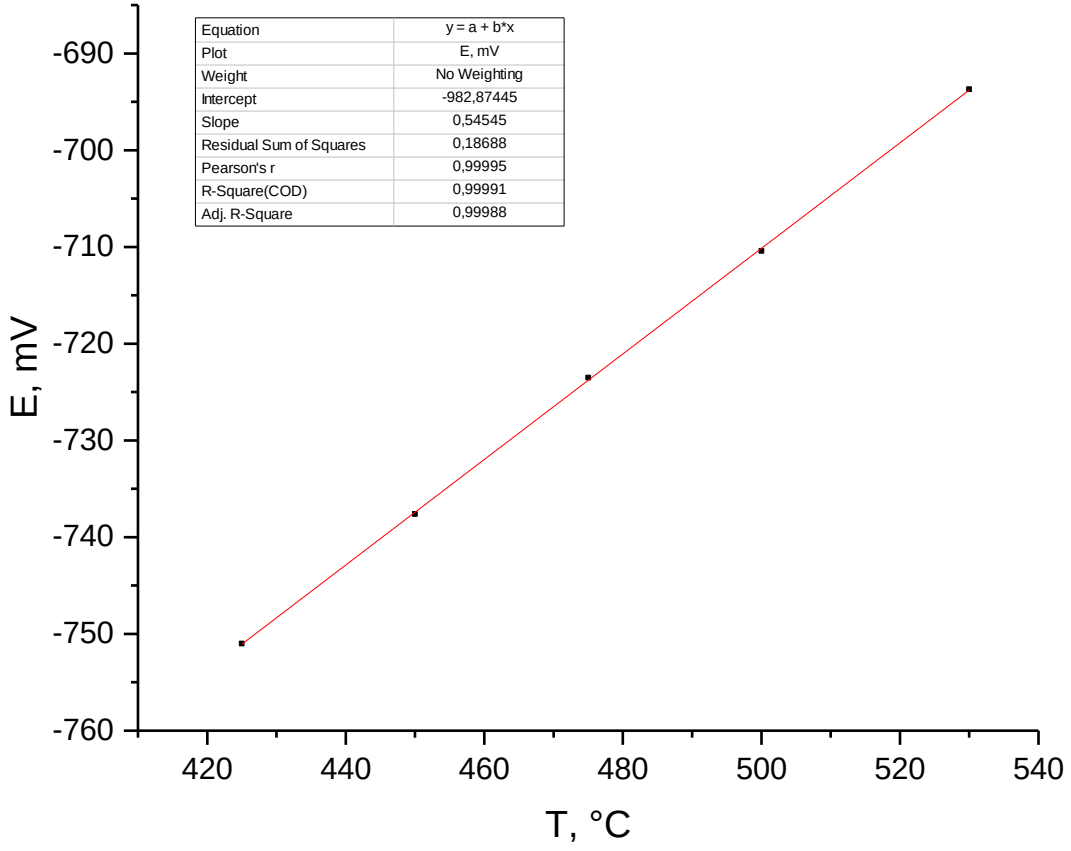

Dependence of the EMF of the sensor on the basis of the Pb-PbO system with a PbO - based electrical lead

Conclusions

- As a result of the conducted studies, it was proved that the oxide layer on the surface of the molybdenum electrical lead of the Bi/Bi_2O_3 reference electrode significantly worsens the metrological characteristics of the sensor (causes drift of the signal, a sharp change in readings, especially when the sensor is impacted by vibration, and enhances the polarizability of the reference electrode).
- The above negative effects disappear when using the $In\text{-}In_2O_3$ or $Bi\text{-}Fe\text{-}Fe_3O_4$ system as the reference electrode, since molybdenum does not oxidize under these conditions. Another solution of the problem is the use of an oxide–based electrical lead: PbO in the case of the Pb-PbO system, Bi_2O_3 in the case of the $Bi\text{-}Bi_2O_3$ system. The results of joint tests of solid electrolyte oxygen sensors in a gas with a molybdenum electrical lead and electrical lead from Bi_2O_3 in the case of the Bi- Bi_2O_3 system as a reference electrode confirmed the conclusions in practice.
- Using oxygen sensors in gases with Bi/Bi_2O_3 reference electrodes (electrical lead from Bi_2O_3) and Pb/PbO (a PbO electrical lead), the dependences of the Gibbs energy values of the formation of bismuth and lead oxides on temperature (for the temperature range 698-803 K) were obtained.
- The obtained dependences are correlated with high accuracy with the data obtained by foreign and Russian authors.

THANK YOU FOR ATTENTION

Shelemet’ev Vasiliy Mikhailovich

SSC RF - IPPE
Phone: 8 (48439) 9-42-77
E-mail: vshelemetev@ippe.ru

RUSSIAN ACADEMY OF SCIENCES
URAL BRANCH
INSTITUTE OF HIGH
TEMPERATURE ELECTROCHEMISTRY

EQUILIBRIUM POTENTIALS OF LEAD OXIDE(II) IN EQUIMOLAR MIXTURE OF $KCl-PbCl_2$

Pershin P.S., Batukhtin V.P.,
Tkacheva O.Yu., Arkhipov P.A., Zaikov Yu.P.

Yekaterinburg 2018

- <u>The aim of the work:</u>

  Determination of activity and activity coefficients of PbO in an equimolar mixture of potassium and lead chloride depending on the temperature and concentration of the oxide;

  Calculation of the partial and integral thermodynamic functions of PbO dissolution in the KCl-$PbCl_2$ melt.

Galvanic cell for EMF measurements:

$-(GC)Pb|(1-N)\cdot KCl\text{-}PbCl_2+N\cdot PbO|ZrO_2(Y_2O_3)|O_2(1atm)(Pt)+$

Temperature range: 738-863 K

Mole fraction of PbO: from 0,0016 to 0,0732.

Processes in cell:

On lead electrode: $Pb \rightarrow Pb^{2+} + 2\bar{e}$,

On oxygen electrode: $0{,}5O_2 + 2\bar{e} \rightarrow O^{2-}$.

Potential-foming reaction:

$$Pb + 0{,}5O_2 \rightarrow PbO_{sol.} \quad (\text{in } KCl\text{-}PbCl_2)$$

Cell scheme:

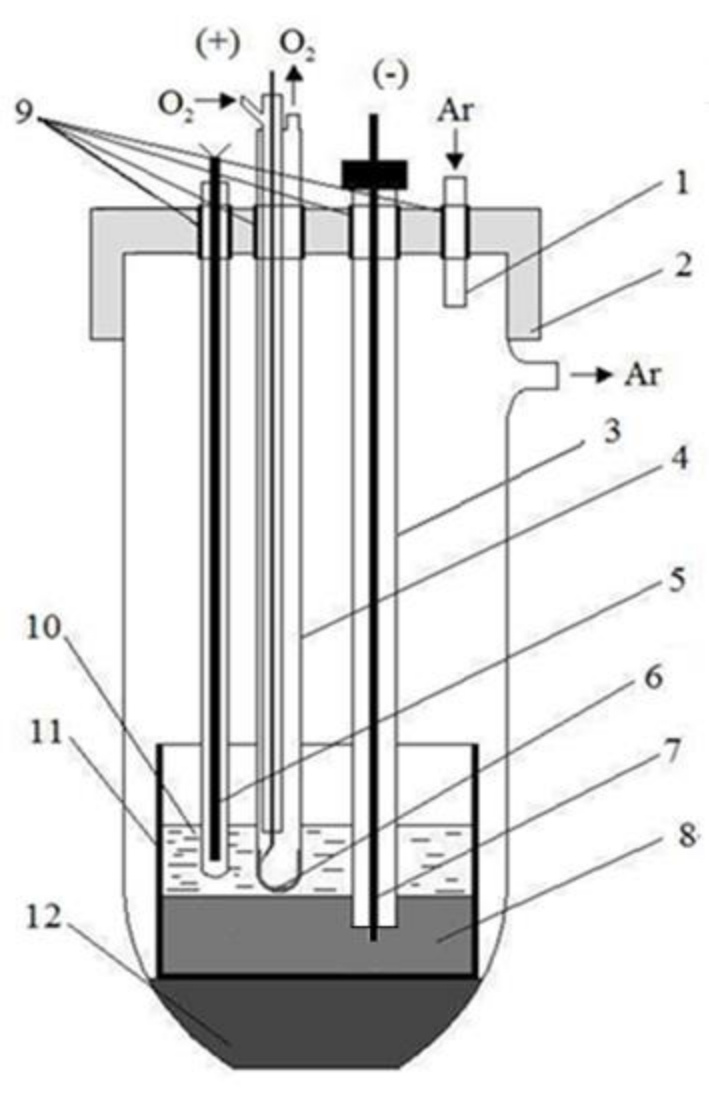

1.- Tube for Ar
2.- Fluoroplastic cover
3.- Alundum tube
4.- Oxygen electrode
5.- Thermocouple Pt-Pt/Rh
6.- Pt-tip
7.- GC lead-current
8.- Pb(liq.)
9.- Technique holes
10.- $KCl-PbCl_2-PbO$ melt
11.- BeO crucible
12.- Fireproof brick

Mole % of PbO	0,16	0,38	0,76	1,56	3,06	5,24	7,32

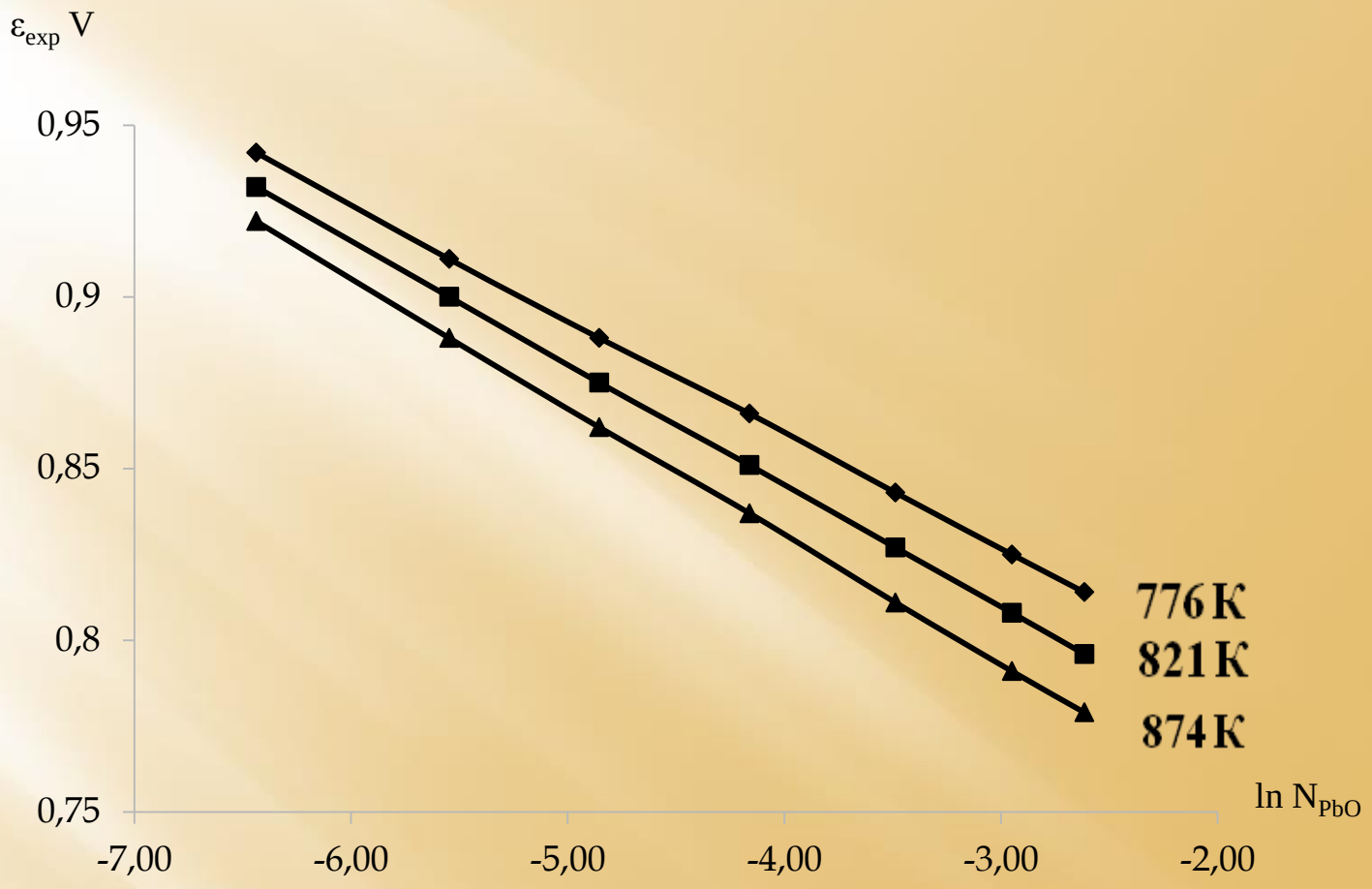

Experimental values of EMF, ε exp

$$\varepsilon_{\text{exp}} = \varepsilon_{\text{temf}} + \varepsilon^{0}_{\text{PbO (liq)}} - \frac{RT}{2F} \ln a_{PbO}$$

TEMF:

T, K	TEMF, mV
776	5,30
821	5,99
874	6,80

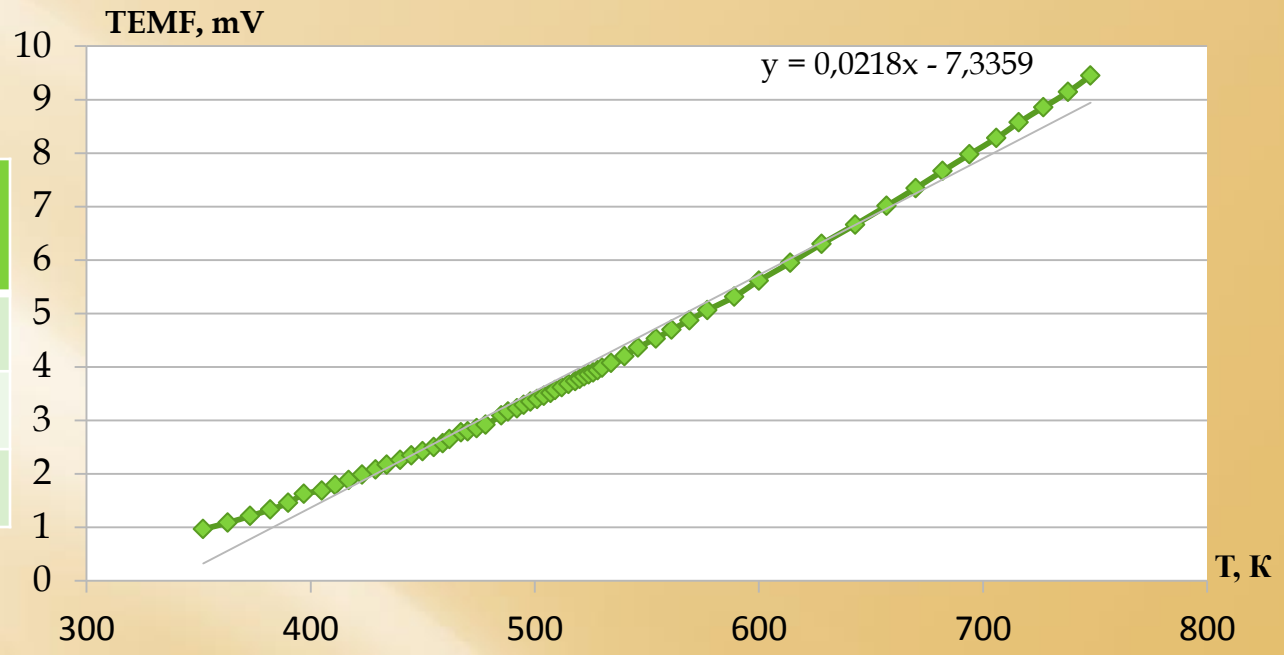

Theoretical voltage of PbO decomposition:

$\Delta_f G^0_{PbO(liq)} = -185497 + 69{,}26 \cdot T$, $J \cdot mole^{-1}$ (1159 – 1775 K),

$\Delta_f G^0_{PbO(liq)} = -2F\varepsilon^0_{PbO(liq)}$

$\varepsilon^0_{PbO\ (liq)} = 0{,}9612 - 0{,}359 \cdot 10^{-3} \cdot T$, V

T, K	$\varepsilon^0_{PbO\ (liq)}$, V
776	0,683
821	0,667
874	0,648

$$\varepsilon = -\frac{RT}{2F}\ln a_{PbO} = \varepsilon_{\text{exp}} - \varepsilon_{\text{temf}} - \varepsilon^{0}_{\text{PbO liq}}$$

The values of experimentally measured EMF (ε exp) and values of EMF (ε) for the calculation of the activity of PbO

$N_{PbO} \cdot 10^2$	776 K		821 K		874 K	
	ε_{exp}	ε_{calc}	ε_{exp}	ε_{calc}	ε_{exp}	ε_{calc}
0,16	0,942±0,003	0,254	0,932±0,004	0,259	0,922±0,001	0,267
0,39	0,911±0,003	0,223	0,900±0,005	0,227	0,888±0,001	0,233
0,78	0,888±0,001	0,200	0,875±0,005	0,202	0,862±0,002	0,207
1,56	0,866±0,001	0,178	0,851±0,002	0,178	0,837±0,001	0,182
3,06	0,843±0,002	0,155	0,827±0,002	0,154	0,811±0,002	0,156
5,24	0,825±0,003	0,137	0,808±0,001	0,135	0,791±0,001	0,136
7,32	0,814±0,002	0,126	0,796±0,001	0,123	0,779±0,001	0,124

Formulas for the calculation

$$a_{PbO} = exp\left[\frac{-2F\varepsilon}{RT}\right]$$

$$\Delta\overline{G}_{PbO_{sol}} = RT \ln a_{PbO_{sol}}$$

$$\gamma_{PbO} = a_{PbO} \cdot N_{PbO}^{-1}$$

$$\Delta\overline{G}_{PbO}^{exc} = RT \ln \gamma_{PbO}$$

The values of ε_{calc} and calculated activities and the coefficients of activity of PbO in the equimolar mixture of KCl-$PbCl_2$ at the temperatures 776K

$N_{PbO} \cdot 10^2$	ε , V	$a_{PbO} \cdot 10^2$	γ_{PbO}	$\Delta\overline{G}_{PbO}$, kJ/mole
0,16	0,254 ± 0,003	0,05 ± 0,01	0,317 ± 0,020	-48,96 ± 0,02
0,39	0,223 ± 0,003	0,13 ± 0,01	0,328 ± 0,020	-42,97 ± 0,08
0,76	0,200 ± 0,001	0,25 ± 0,01	0,326 ± 0,012	-38,54 ± 0,07
1,56	0,178 ± 0,001	0,49 ± 0,02	0,315 ± 0,023	-34,29 ± 0,10
3,06	0,155 ± 0,002	0,98 ± 0,01	0,320 ± 0,012	-29,85 ± 0,03
5,24	0,137 ± 0,003	1,68 ± 0,03	0,320 ± 0,003	-26,38 ± 0,03
7,32	0,126 ± 0,002	2,33 ± 0,03	0,318 ± 0,007	-24,26 ± 0,06

The values of ε_{calc} and calculated activities and the coefficients of activity of PbO in the equimolar mixture of KCl-$PbCl_2$ at the temperatures 821 K

$N_{PbO} \cdot 10^2$	ε , B	$a_{PbO} \cdot 10^2$	γ_{PbO}	$\Delta\overline{G}_{PbO}$, kJ/mole
0,16	0,259 ± 0,004	0,07 ± 0,01	0,413 ± 0,016	-49,98 ± 0,46
0,39	0,227 ± 0,005	0,16 ± 0,01	0,419 ± 0,016	-43,81 ± 0,01
0,76	0,202 ± 0,005	0,33 ± 0,01	0,424 ± 0,010	-38,98 ± 0,11
1,56	0,178 ± 0,002	0,65 ± 0,01	0,418 ± 0,021	-34,35 ± 0,06
3,06	0,154 ± 0,002	1,29 ± 0,01	0,420 ± 0,012	-29,72 ± 0,05
5,24	0,135 ± 0,001	2,20 ± 0,01	0,420 ± 0,003	-26,05 ± 0,04
7,32	0,123 ± 0,001	3,09 ± 0,01	0,422 ±0,003	-23,74 ± 0,07

The values of ε_{calc} and calculated activities and the coefficients of activity of PbO in the equimolar mixture of KCl-$PbCl_2$ at the temperatures 863 K

$N_{PbO} \cdot 10^2$	ε , B	$a_{PbO} \cdot 10^2$	γ_{PbO}	$\Delta\overline{G}_{PbO}$, kJ/mole
0,16	0,267 ± 0,001	0,08 ± 0,01	0,518 ± 0,019	-51,56 ± 0,21
0,39	0,233 ± 0,001	0,20 ± 0,03	0,524 ± 0,063	-45,00 ± 0,10
0,76	0,207 ± 0,002	0,41 ± 0,02	0,523 ± 0,028	-39,98 ± 0,39
1,56	0,182 ± 0,001	0,79 ± 0,06	0,508 ± 0,056	-35,16 ± 0,04
3,06	0,156 ± 0,002	1,58 ± 0,07	0,516 ± 0,035	-30,14 ± 0,04
5,24	0,136 ± 0,001	2,69 ± 0,13	0,513 ± 0,023	-26,28 ± 0,01
7,32	0,124 ± 0,001	3,69 ± 0,12	0,505 ± 0,017	-23,97 ± 0,09

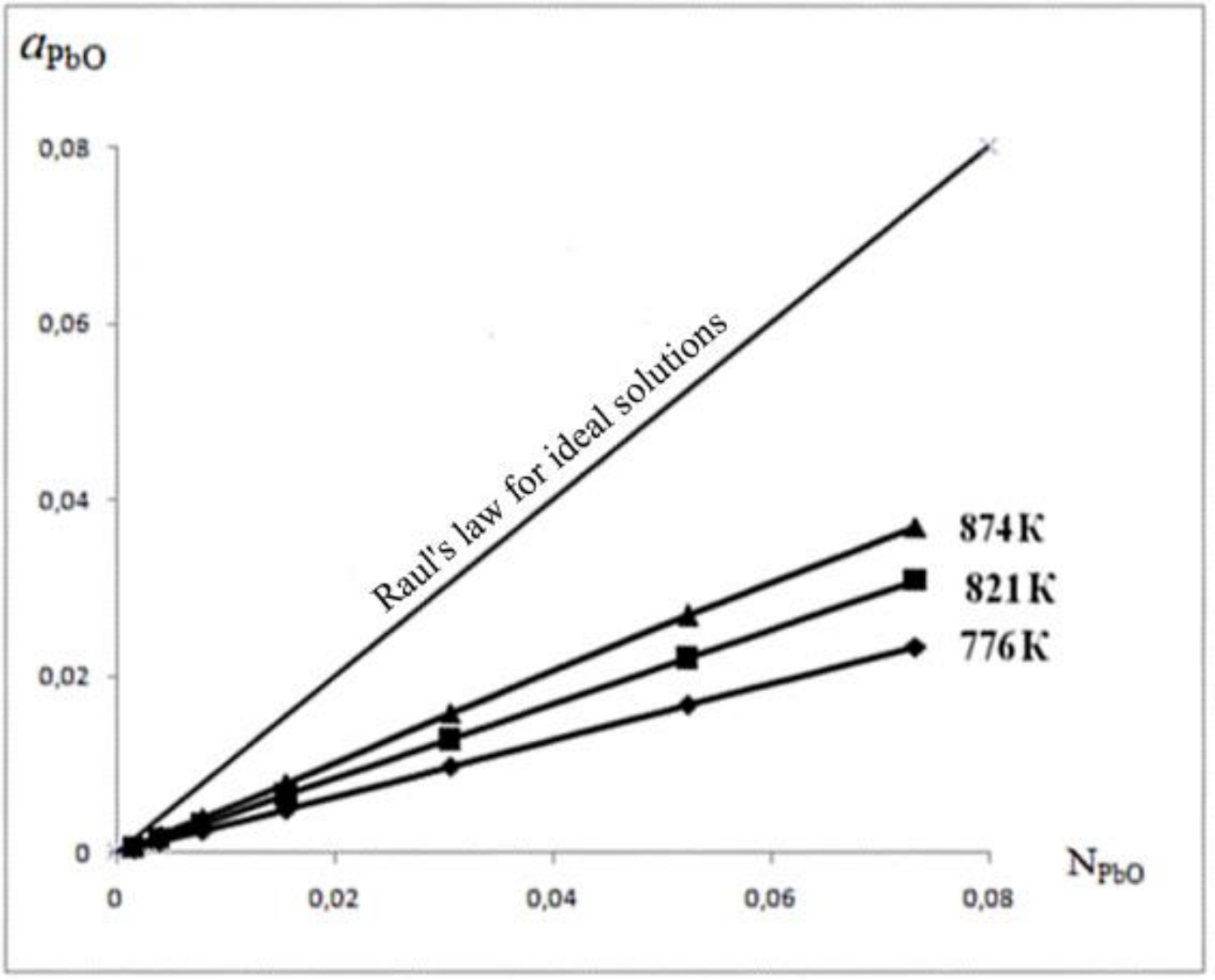

Dependence of activity of PbO on temperature and PbO concentration

T, K	776	821	874
γ_{PbO}	0,321	0,419	0,515
$\Delta\overline{G}^{exc}_{PbO}$ kJ/mole	-7,34	-5,60	-4,82

Values of partial molar entropy and enthalpy for PbO in solution

$N_{PbO}\cdot 10^2$	$\Delta\overline{S}_{PbO}$ J/mole·K	$\Delta\overline{H}_{PbO}$ kJ/mole
0,16	-26,68	-28,19
0,39	-20,73	-26,85
0,76	-14,89	-26,90
1,56	-9,05	-27,15
3,06	-3,10	-27,35
5,24	0,83	-26,92
7,32	2,74	-26,24

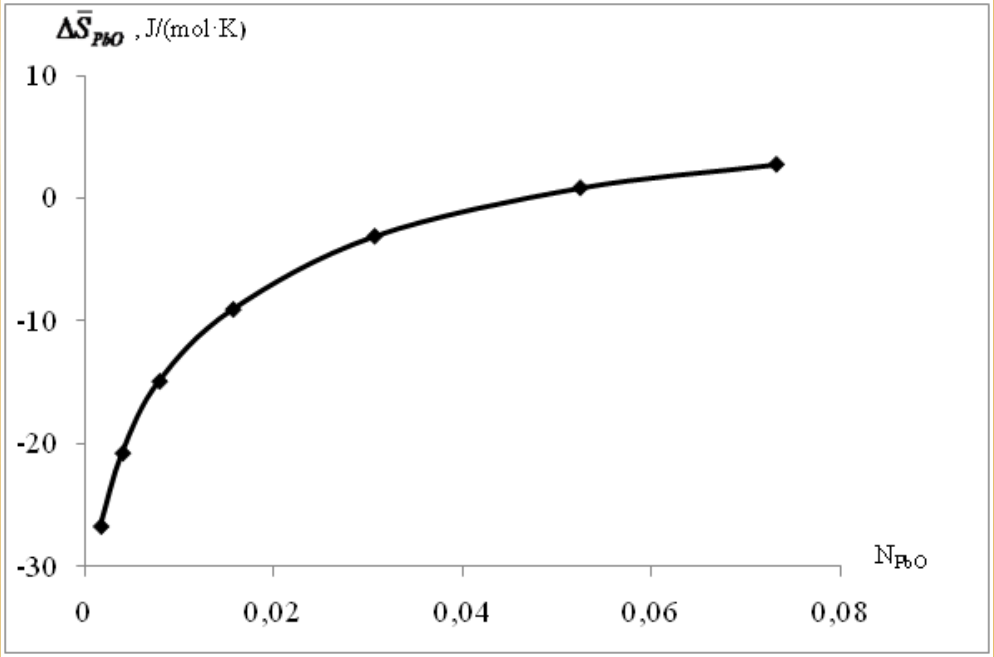

Dependence of partial molar entropy on concentration of PbO

$$a_R = N_R \qquad \Delta\overline{G}_R = RT \cdot \ln N_R$$

$$\Delta G = N_{PbO} \cdot \Delta\overline{G}_{PbO} + \left(1 - N_{PbO}\right) \cdot \Delta\overline{G}_R$$

Integral Gibbs energy (-ΔG, kJ/mol) for dilute solutions

T, K	Мол.% PbO в растворе						
	0,16	0,38	0,76	1,56	3,06	5,24	7,32
776	0,089	0,193	0,351	0,635	1,108	1,711	2,230
874	0,094	0,204	0,368	0,661	1,141	1,748	2,266

Partial entropy and enthalpy of the solvent ($KCl\text{-}PbCl_2$) = R and integral entropy and enthalpy of the solution ($KCl\text{-}PbCl_2$)+ PbO:
and in J/mol·K; and in J/mol

$N_R \cdot 10^2$	99,84	99,62	99,24	98,44	96,94	94,76	92,68
$\Delta\overline{S}_R$	0,0133	0,0325	0,0651	0,1307	0,2584	0,4475	0,6320
$\Delta\overline{H}_R$	0,022						
ΔS	-0,029	-0,048	-0,052	-0,013	0,156	0,468	0,786
ΔH	-45	-105	-210	-423	-837	-1411	-1921

$$2Pb^{2+} + O^{2-} + Cl^{-} = Pb_2OCl^{+}$$

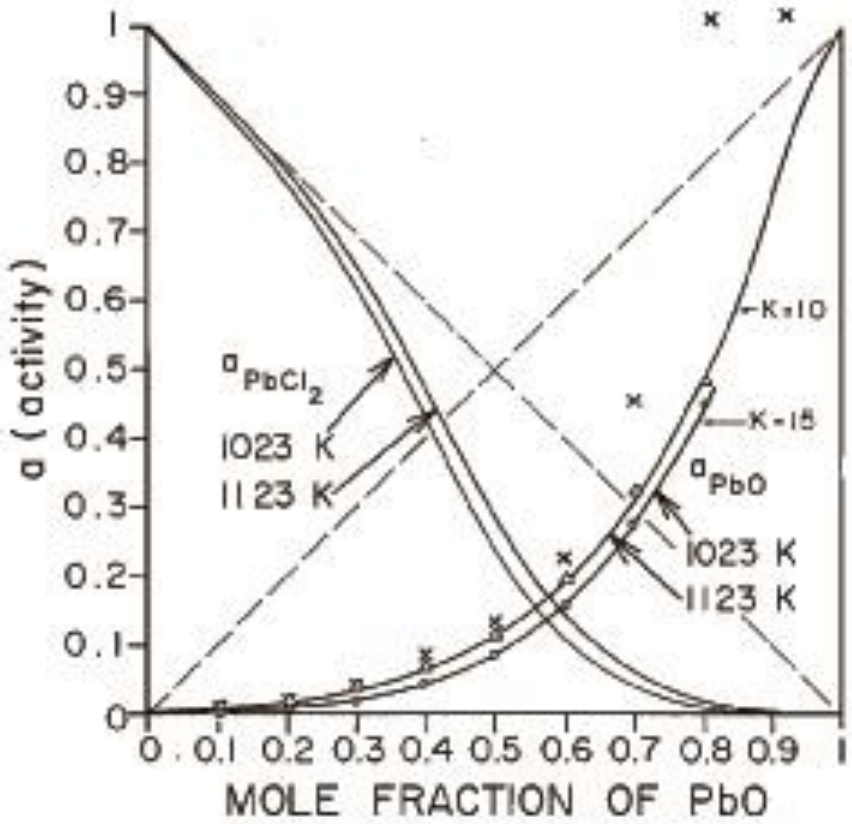

FIG. 2. Activity isotherms for PbO and $PbCl_2$ at 1023 K and 1123 K.

Flengas S.N., Hacetoglu A. Thermodynamic behavior of molten metal oxychlorides: the PbO-$PbCl_2$ system. Can. J. Chem. 1990, v. 68,p. 236-242.

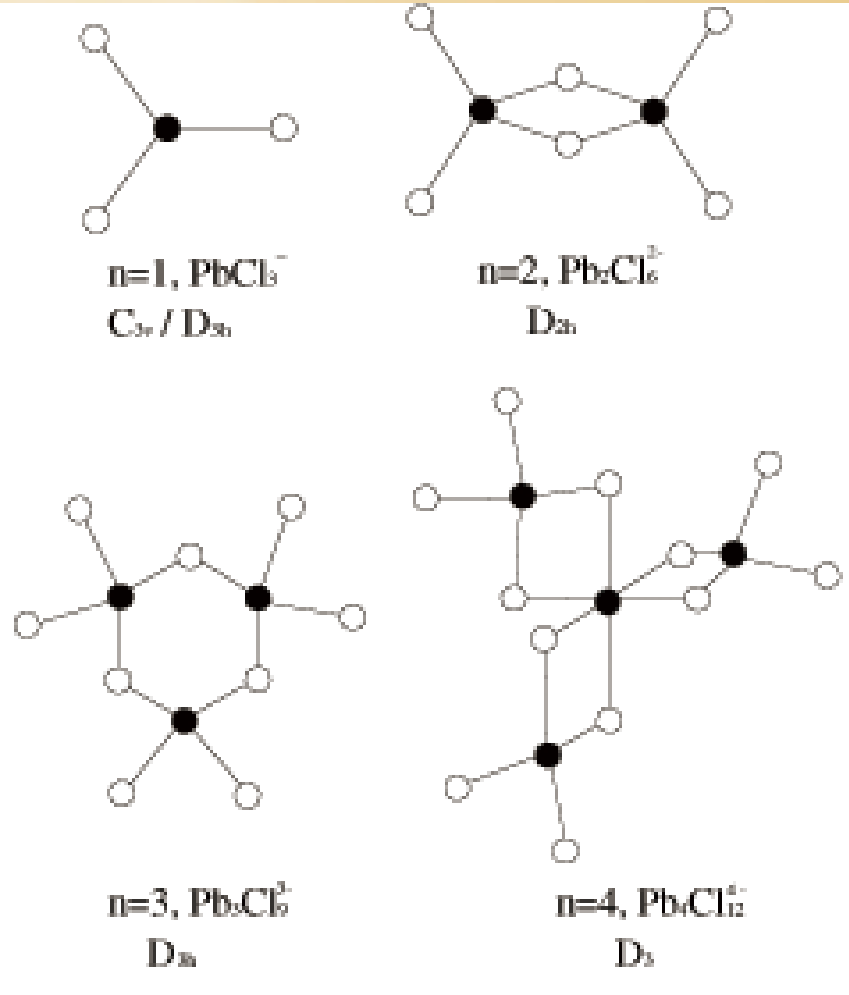

Dracopoulos V., Kastrissios D.Th., Papatheodorou G.N. Raman spectra and structure of PbCl2–ACl (A = K, Cs) melts. Polyhedron, 24 (2005) p. 619–625.

- Thus, there is probably equilibrium between chloride complexes in the solvent $KCl\text{-}PbCl_2$:

$$3(KCl\text{-}PbCl_2) \rightarrow \{3K^+[Pb_3Cl_9]^{3-}\} \leftrightarrow \{2K^+[Pb_2Cl_6]^{2-}\} + \{K^+[PbCl_3]^-\}$$

- The dissolution of the solid PbO in the chloride melt is assumed to be presented as follows:
  - $\{3K^+ + [Pb_3Cl_9]^{3-}\} + 2PbO \rightarrow$
  - $[Cl_2Pb\text{-}O\text{-}PbCl_2]^{2-} + [PbCl_3]^- + 3K^+ + [ClPb\text{-}O\text{-}PbCl]^o$

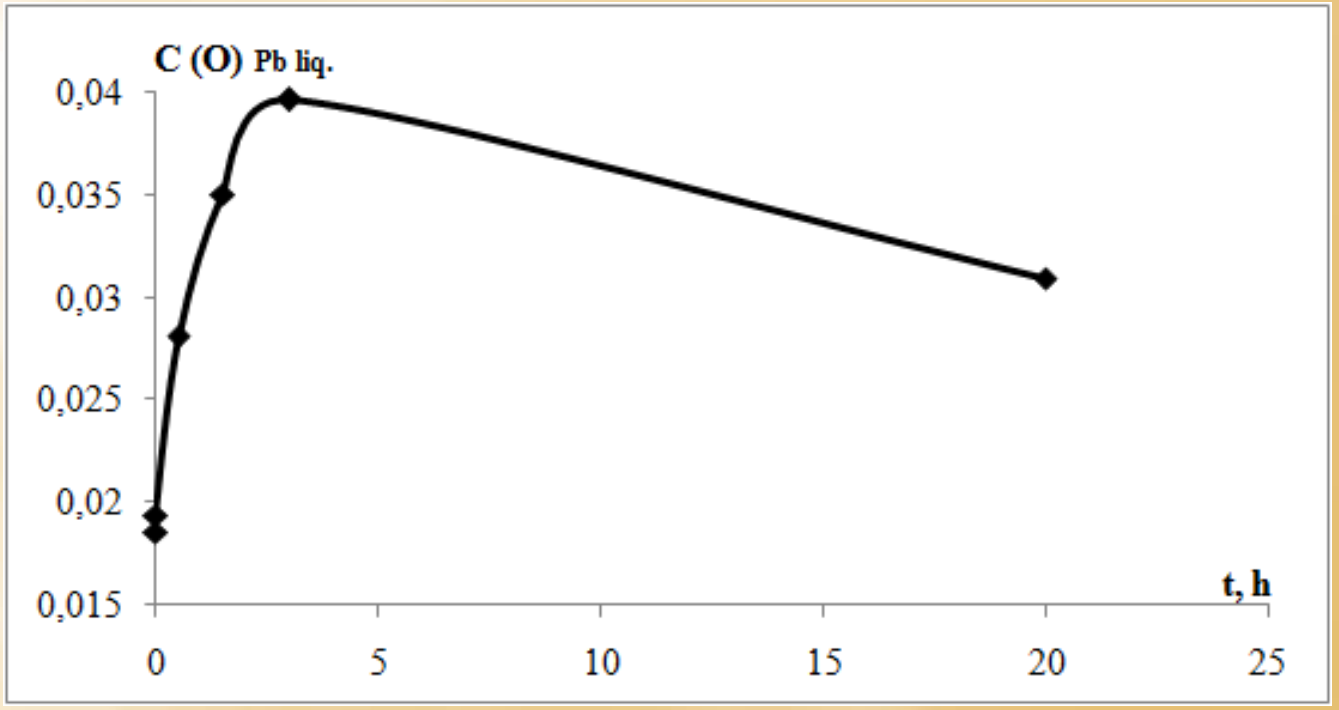

Change in oxygen concentration in molten lead, wt.%

Conclusions :

The EMF method was used to measure the equilibrium potentials of the liquid metallic lead relatively to the solid electrolyte membrane oxygen electrode in the KCl-$PbCl_2$+PbO melt depending on the PbO concentration at the temperatures 776, 821 and 874 K.

From the experimental values of the EMF activities, the coefficients of activity and partial and integral thermodynamic functions of the components were calculated.

The moderate negative deviations of the activity of PbO in the KCl-$PbCl_2$ equimolar mixture from the ideal solution's law were established.

Thank you for your Attention!